ACS OMEGA

http://pubs.acs.org/journal/acsodf

Article

Insights into Selective Removal by Dye Adsorption on Hydrophobic vs Multivalent Hydrophilic Functionalized MWCNTs

José Arévalo-Fester and Alexander Briceño*

Cite This: *ACS Omega* 2023, 8, 11233−11250

Read Online

ACCESS | Metrics & More | Article Recommendations

ABSTRACT: Hydrophilic functionalized carbon nanotubes (MWCNT-COOH) were developed via hydrothermal glucose-coated carbonization, mixing MWCNTs with glucose in different weight ratios. Methyl violet (MV), methylene blue (MB), alizarin yellow (AY), and methyl orange (MO) were used as dye models for adsorption studies. Comparative dye adsorption capacity onto the pristine (MWCNT-raw) and functionalized (MWCNT-COOH-11) CNTs was evaluated in aqueous solution. These results revealed that MWCNT-raw is capable of adsorbing either anionic or cationic dyes. In contrast, an induced selective cation dye adsorption capacity is significantly enhanced on multivalent hydrophilic MWCNT-COOH, in comparison to a pristine surface. This ability can be tuned to the selective adsorption of cations over anionic dyes or between anionic mixtures from binary systems. An insight into adsorbate−adsorbent interactions shows that hierarchical supramolecular interactions dominate the adsorption processes, which is ascribed to the chemical modification by switching from a hydrophobic to a hydrophilic surface, dye charge, temperature, and potential matching multivalent acceptor/donor capacity between chemical groups in the adsorbent interface. The dye adsorption isotherm and thermodynamics on both surfaces were also studied. Changes in the Gibbs free energy ($\Delta G°$), enthalpy ($\Delta H°$), and entropy ($\Delta S°$) were evaluated. Thermodynamic parameters were endothermic on MWCNT-raw, whereas the adsorption process on MWCNT-COOH-11 revealed that adsorption processes were spontaneous and exothermic, accompanied by a significant reduction of entropy values as a consequence of a multivalent effect. This approach provides an eco-friendly, low-cost alternative for the preparation of supramolecular nanoadsorbents with unprecedented properties to achieve remarkable selective adsorption independent of the presence of intrinsic porosity.

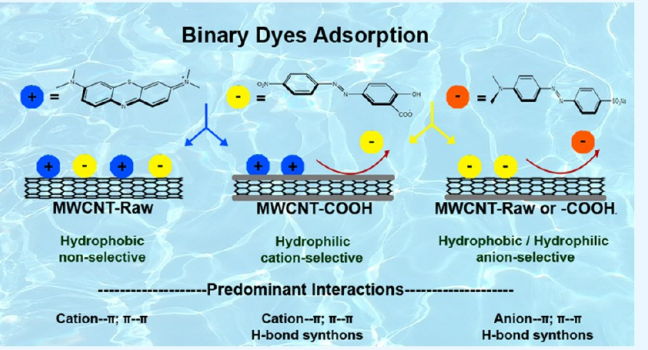

INTRODUCTION

In recent years, supramolecular chemistry concepts have been extended to molecular recognition directed at surfaces,[1−3] allowing access to sophisticated and ingenuous tailor-made design of novel selective receptors and/or adsorbents from molecular/nanoscale material to bulk scale technologies via bottom-up and top-down approaches.[4−7] Thus, deliberate surface functionalization provides an exciting route to engineer supramolecular solid materials with distinctive adsorption performance,[8−10] leading to novel possibilities in diverse fields related to molecular and/or metallic sensing, selective adsorption process, and/or separation of a complex mixture of molecules, such as multistep adsorption processes owing to a tunable surface in each adsorption step via layer-by-layer formation[11,12] as well as enantiomeric mixed separation based on supramolecular recognition modes.[13,14] This alternative provides the following additional advantages over traditional adsorbents: (a) Such surfaces can be tuned to discriminate molecular and/or metallic adsorption components, and as a consequence, the possibility of incorporating either acidic or basic sites on the surface.[15−17] (b) It is possible to achieve high adsorption capacity even with a lack of intrinsic porosity, simply directed by supramolecular surface recognition.[18−21] (c) This alternative provides interesting chemical groups that are able to drive a selective adsorption process via complementary classical hierarchical supramolecular synthons between the substrate−adsorbate, which may be controlled by a careful choice of the interaction strength and the combination of multiple interactions (multivalency) into a single material. In these surfaces, the adsorption capacity is favored by cooperative effects, leading to a greater affinity of the adsorbate on the interface.[22−24]

Recently, in our previous research, a comprehensive interpretation from a supramolecular perspective for the selective removal by adsorption of cationic dyes vs anionic

Received: December 27, 2022
Accepted: February 27, 2023
Published: March 9, 2023

Name	Structure	Mw ($g \cdot mol^{-1}$)	λ_{Max} UV-Vis (nm)	pKa	Solubility ($mg \cdot mL^{-1}$)
Methylene Blue	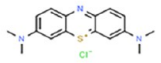	319.8	665	3.14	50
Methyl Violet	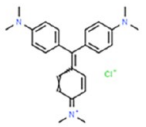	407.97	580	1.7	>850
Methyl Orange	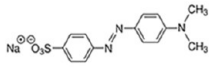	327.33	464	3.4	500
Alizarin Yellow	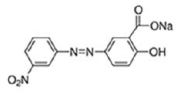	309.21	362	11.2	12

Figure 1. Chemical molecular structures of the organic dyes evaluated for the adsorption processes, showing chemical groups able to interact with the different surfaces and their physicochemical properties.

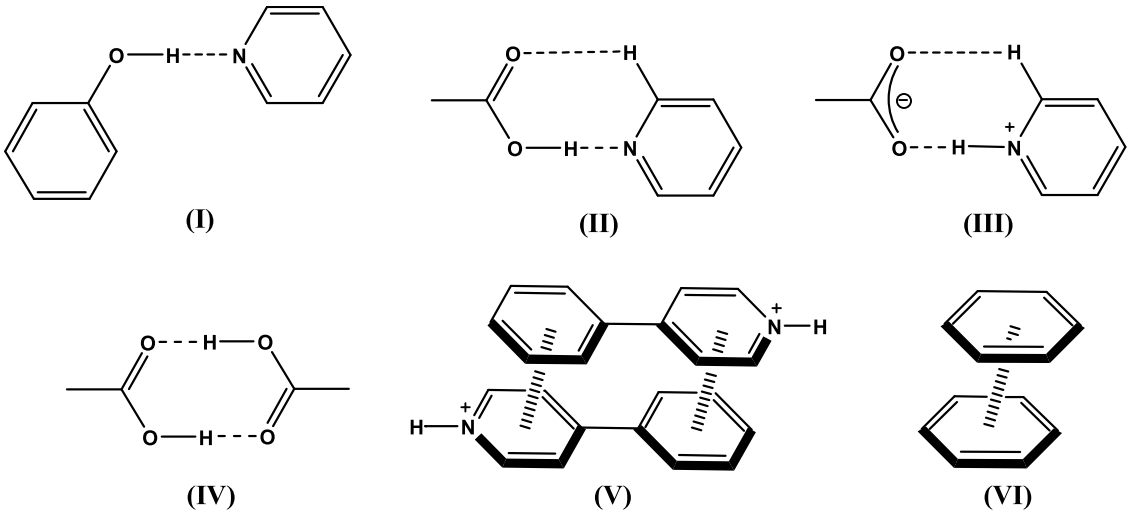

Figure 2. Chemical molecular structures of recognized supramolecular synthons based on hydrogen bonding synthons (I–IV), cation–π, and π–π interactions (V–VI).

dyes on pristine and functionalized carbon-sorbent surfaces was successfully reported.[20] We have also demonstrated that the adsorption processes are directed by hydrogen bond synthons, and such interactions are recognized by their strength and directionality.[20,21] In this context, continuing ongoing studies on the use of hydrophilic/hydrophobic carbon solid platforms as potential templates and/or selective adsorbents in combination with our studies on the use of multivalent interactions in the crystal engineering field (Figure 1),[25,26] herein we have extended this approach to evaluate dye adsorption directed by surface recognition on two distinctive carbon-sorbent surface models.

The conventional route for functionalization of carbon surfaces consists of grafting oxygenated moieties via chemical oxidation, generating distinctive hydrophilic groups (e.g., carboxylic, epoxide, hydroxyl, quinines, among others). Usually, for this, chemical modifications used strong and hazardous oxidants (e.g., inorganic acids, chlorates, $KMnO_3$, etc.). Thus, alternative eco-friendly approaches for the functionalization of carbon materials are of great synthetic significance.[9,20,21]

In this case, the use of carbohydrates for functionalization is an alternative cheaper, simpler, and safer, as well as, the final disposal of resulting filtrates. In this contribution, pristine CNTs were modified by one-pot hydrothermal carbonization treatments[27−29] using glucose as the oxygenated functional group precursor,[30,31] producing samples with differentiated surface chemistry and textural parameters, leading to hydrophilic nanotubes (MWCNT-COOH). Such CNTs were evaluated for the study of either a cationic or an anionic dye adsorption process (Figure 1). Comparative dye adsorption studies onto both CNTs revealed important insights into the adsorption behavior on the distinctive surfaces. Preferential and selective dye adsorption can be switched, depending on the hydrophobicity/hydrophilicity of the surface, charge, and potential multivalent acceptor/donor capacity of the dye onto the surface.

Furthermore, Langmuir, Freundlich, and Temkin adsorption isotherms were studied to explain the sorption mechanism.[32] Thus, we have recognized and characterized two kinds of supramolecular domains based on potential noncovalent interactions. The adsorption process on hydrophilic MWCNT-COOH is directed by surface recognition based on directional and robust hydrogen bond supramolecular synthons:[33−37] pyridine–carboxylic acid, O–H···N, cation···π,

https://doi.org/10.1021/acsomega.2c08203
ACS Omega 2023, 8, 11233−11250

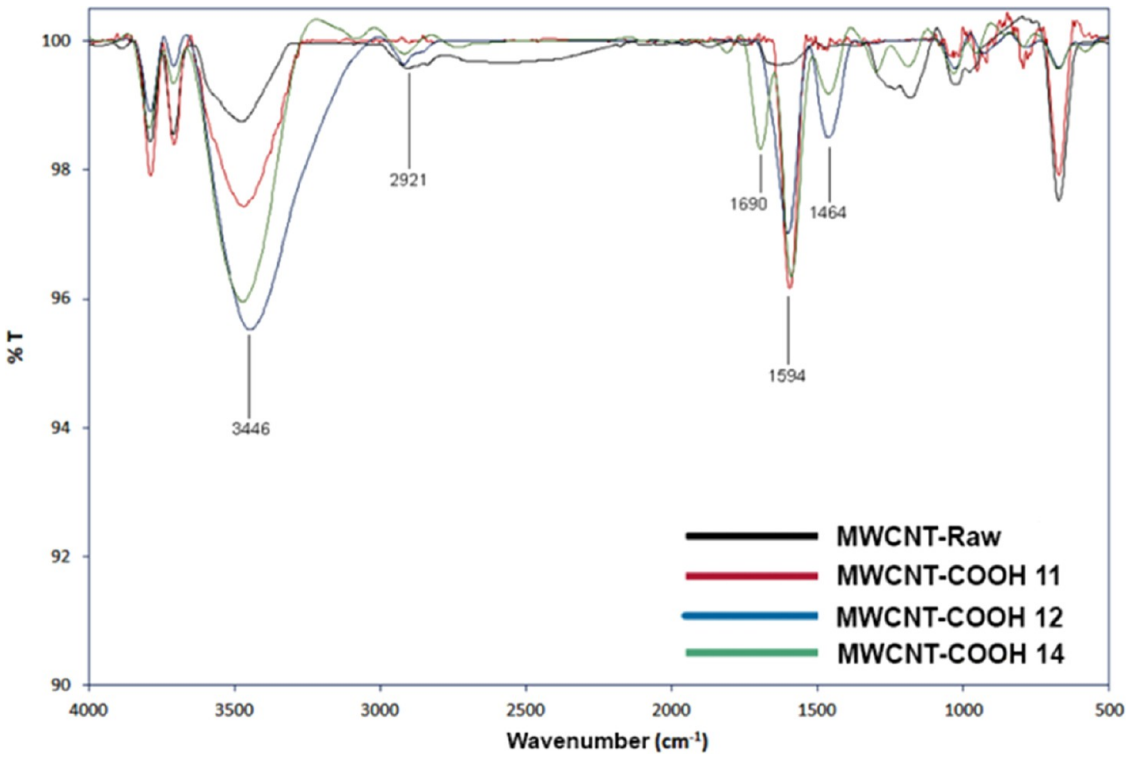

Figure 3. FT-IR spectrum of MWCNT-raw and functionalized MWCNT-COOH (-11, -12, and -14).

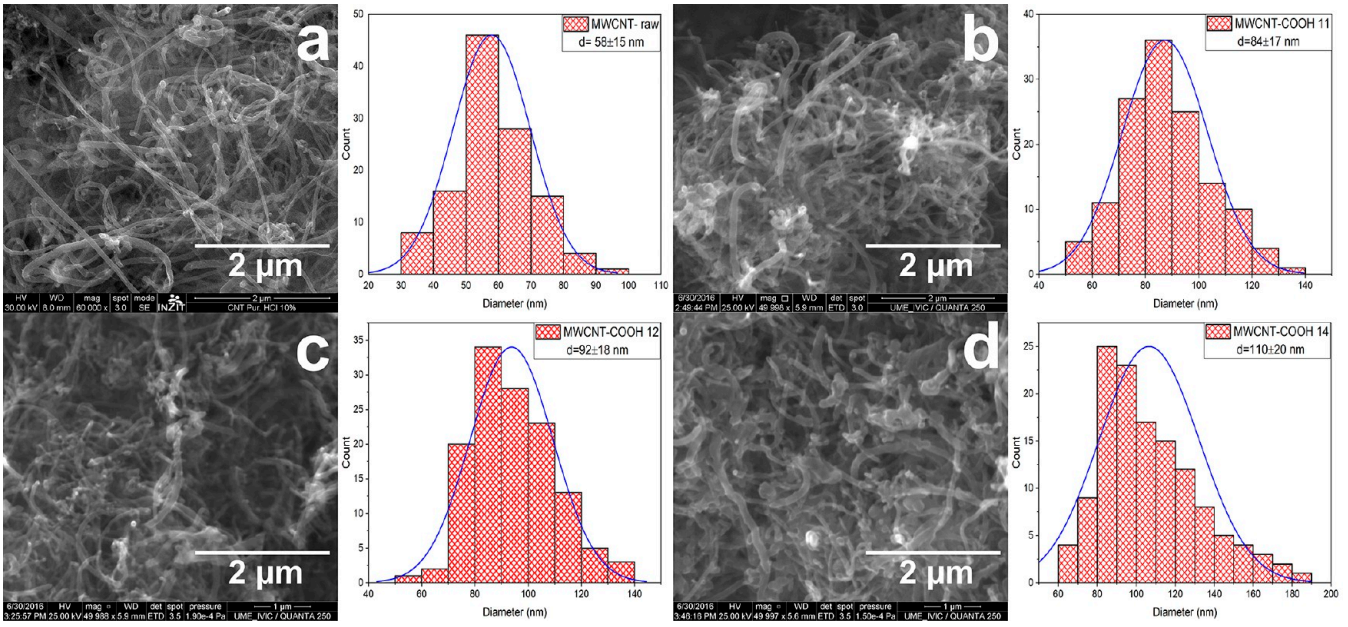

Figure 4. SEM micrographs of MWCNT-raw (a) and functionalized MWCNT-COOH-11, -12, and -14 (b–d).

$\pi\cdots\pi$, and electrostatic interactions (Figure 2), whereas an adsorption process on MWCNT-raw is controlled almost exclusively by cation$\cdots\pi$, $\pi\cdots\pi$, and ionic interactions in comparison to hydrophilic platforms.

RESULTS AND DISCUSSION

Functionalization of CNTs Pristine (MWCNT-Raw) under Hydrothermal Conditions and Characterization of MWCNT-Raw and Functionalized MWCNT-COOH. The surface of MWCNT-raw was modified via hydrothermal glucose-coated carbonization, leading to hydrophilic surface nanotubes (MWCNT-COOH). This approach should provide different and abundant oxygenated groups on the surface more than conventional oxidation with mineral acids.[38,39] Figure 3 displays Fourier-transform infrared (FT-IR) spectra of the CNTs glucose-coated with 1:1,1:2, and 1:4 CNT/glucose weight ratios (MWCNT-COOH-11, MWCNT-COOH-12, and MWCNT-COOH-14). As expected, FT-IR spectra analysis revealed that the variation of glucose concentrations produced a gradual increment of some absorption bands related to the presence of oxygenated groups on the surface. Specifically, an increment was observed in the relative intensity of the bands due

https://doi.org/10.1021/acsomega.2c08203
ACS Omega 2023, 8, 11233−11250

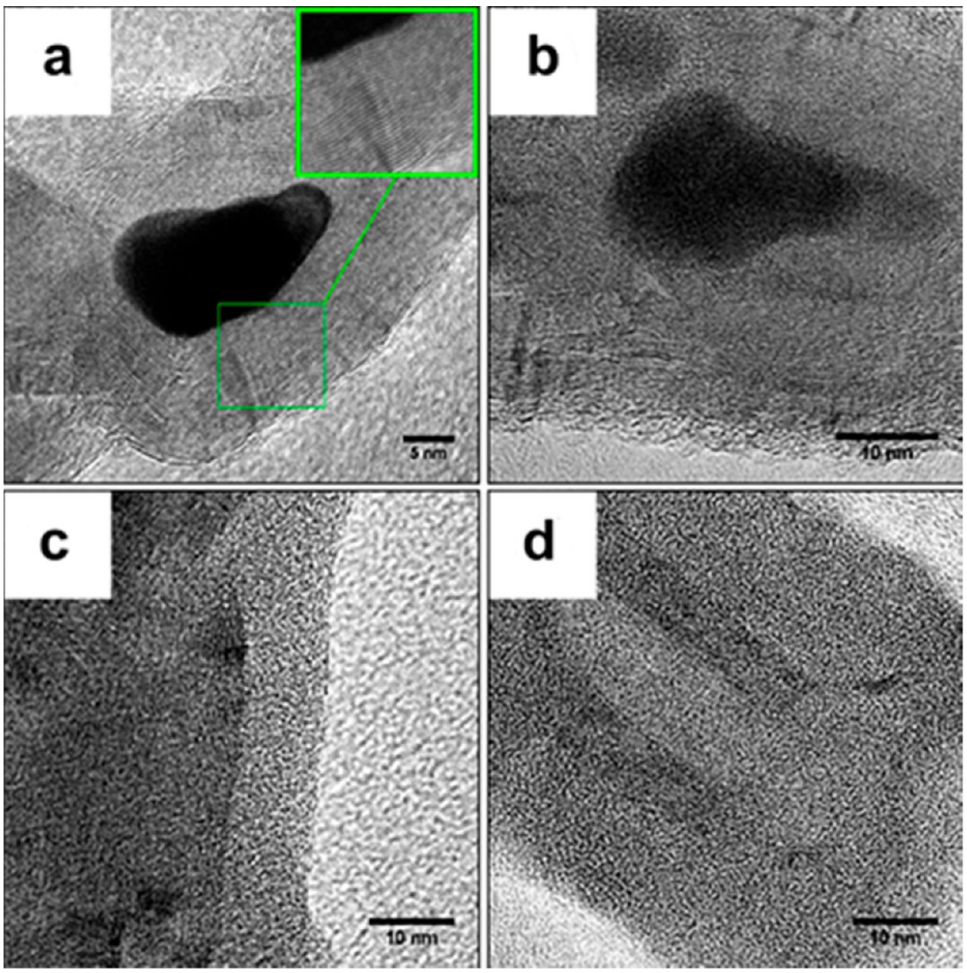

Figure 5. HRTEM (inset) micrographs of pristine MWCNT-raw (a) and functionalized MWCNT-COOH-11, -12, and -14 (b−d).

to O−H (3000−3500 cm^{-1}) and C═O and C−O groups at 1690 and 1463 cm^{-1}, respectively.

The resulting solids were analyzed by scanning electron microscopy (SEM), to evaluate the effect of glucose on possible morphological changes of CNTs. Figure 4 shows SEM micrographs of pristine and functionalized MWCNT-COOH (-11, -12, and -14). The CNTs' morphologies were not evidently altered after the hydrothermal treatment. Likewise, these images revealed the formation of characteristic hydrophilic carbon spheres observed from simple hydrothermal carbonization of carbohydrates for the solid obtained from a 1:4 ratio.

Comparative analysis of the diameter estimation of MWCNT-raw and functionalized reveals an increase of the average diameter value with the increase of the glucose molar ratio from 58.3 nm for MWCNT-raw up to 84.6 and 110.4 nm for MWCNT-COOH-11, 12, and 14.

The high-resolution electron microscopy (HRTEM) micrographs of MWCNT-raw (Figure 5a) show no structural defects, and the existence of insignificant amounts of amorphous carbon and individual catalyst particles was noticed. The outer tube diameter of the pristine CNTs is 38.6 nm with a length in the range of 7−10 μm. The internal diameter of the wall is between 5.8 and 7.6 nm. These micrographs show a highly ordered graphitic layer, and the (002) lattice fringes are observed to be axially parallel with one another with a total of 31 layers of walls arranged concentrically (inset). The estimated plane-to-plane distance between the walls derived from the FFT result is 0.335 nm, which is in agreement with the nominal distance between the planes in crystalline CNTs.

Figure 5b−d shows the HRTEM micrographs of functionalized MWCNT-COOH-11, -12, and -14. These images show the preservation of their tubular shape with an increase of the outer diameter when varying the CNTs/glucose ratio (49.6 and 75.4 nm, respectively).

The HRTEM micrograph revealed that these values of diameters are related to the presence of a coated amorphous carbon layer covering the CNT core, which becomes thicker with the increase of glucose in the reaction media from 3.2 nm MWCNT-COOH-11 to 14.4 nm for MWCNT-COOH-14. The amorphous layer is rich in oxygenated groups (−OH, −COOH, −C═O) as determined by FT-IR.

To evaluate quantitatively the functionalization degree of the hydrothermally treated vs pristine CNTs, the Boehm titration method was employed,[38] and the corresponding results are shown in Table 1. These results are in agreement with the

Table 1. Total Acidic and pH_{pzc} Values for Pristine and Functionalized MWCNT-COOH-11, -12, and -14

carbon sample	total acidic groups (mmol mg^{-1})	pH_{pzc}
MWCNT-raw	4.1 ± 1.3	8.0
MWCNT-COOH-11	22.5 ± 1.0	2.9
MWCNT-COOH-12	22.9 ± 0.8	3.0
MWCNT-COOH-14	21.8 ± 1.2	2.9

https://doi.org/10.1021/acsomega.2c08203
ACS Omega 2023, 8, 11233−11250

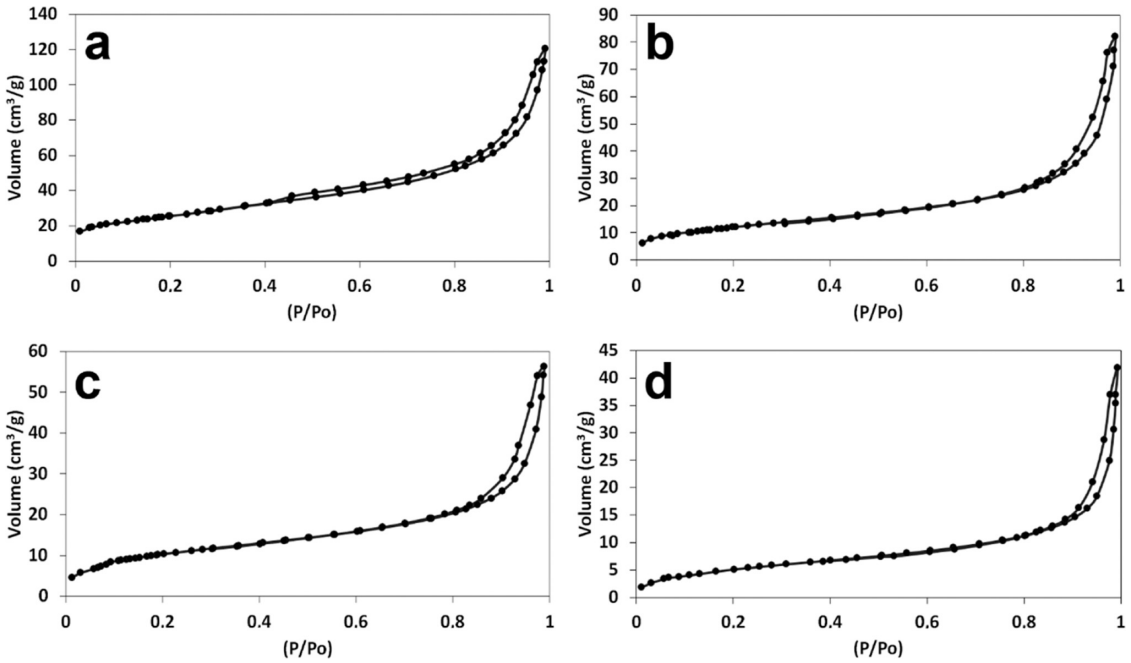

Figure 6. N_2 adsorption−desorption isotherms of pristine MWCNT-raw (a) and functionalized MWCNT-COOH-11, -12, and -14 (b−d).

evidence of the presence of oxygen functionalities provided by FT-IR spectroscopy. The total acidity of the MWCNT-COOH increased by a factor of ≈5-fold in comparison to the pristine surface. To our surprise, this value did not vary statistically with the increase of the glucose amount, obtaining an average value of 22 ± 1 mmol mg^{-1}.

These results indicate that a controllable functionalization process can be attained under mild conditions using glucose as a green oxidant. This possibility provides an interesting eco-friendly alternative to induce chemical incorporation of oxygenated moieties on the surface of a given carbonaceous material in comparison to conventional oxidation methods.[38,39] Further evidence for the efficiency of induced hydrothermal oxidation was provided by the point of zero charge (pH_{pzc}) measurements by the pH-drift method,[40] and the surface acidic group determination of the adsorbents was determined according to the Boehm titration.[41] Table 1 compares the pH_{pzc} values of the raw and hydrothermally functionalized CNTs at different glucose concentrations. These values gradually become more acidic from a slightly basic pH_{pzc} of 8.00 for MWCNT-raw to ≈3.00 for MWCNT-COOH, due to the increasing concentration of the covalently functionalized surface with acidic groups and is consistent with the presence of hydrophilic groups as potential anchoring sites able to interact with self-complementary chemical groups of the dyes.

Surface Area Measurements. The nitrogen adsorption−desorption isotherms of all of the CNTs can be categorized as type IV(b) with H_3-type hysteresis loops at high $P/P_o > 0.8$, in agreement with the original IUPAC nomenclature.[42] However, according to the extended classification of adsorption isotherms according to Rouquerol,[43] the isotherms are classified as type IIb isotherms, characteristic of nonporous or macroporous aggregate powders (Figure 6). Table 2 shows the values corresponding to the S_{BET}, volume pore, and pore diameter of the raw and hydrothermally functionalized CNTs subjected to different glucose amounts.

A gradual decrease in the apparent S_{BET} values is observed in these solids with increasing glucose weight ratios, which vary in the range of 91−23 m^2 g^{-1}. This behavior is associated with the size of particle growth due to the coated layer on functionalized CNTs. A similar trend is observed with the average pore volume values in the range of 0.16−0.02 cm^3 g^{-1}.

Table 2. N_2 Sorption-Derived Textural Properties of Pristine and Functionalized MWCNT-COOH-11, -12, and -14

	textural properties		
sample	S_{BET} (m^2 g^{-1})	V_p (cm^3 g^{-1})	D_{BJH} (nm)
MWCNT-raw	91	0.16	10
MWCNT-COOH-11	44	0.11	14
MWCNT-COOH-12	38	0.08	13
MWCNT-COOH-14	23	0.02	12

Thermogravimetric analysis (TGA) of the adsorbent samples is shown in Figure 7. TGA of MWCNT-raw shows the highest thermal stability with an oxidation peak at 665 °C, and this value is characteristic in CNTs with a high degree of crystallinity and low amount of residual catalyst particles. A gradual decrease of the thermal stability of the functionalized MWCNT-COOH is observed with respect to MWCNT-raw with increasing glucose concentrations. These materials show weight losses in the temperature range of 300 to 600 °C, which is in agreement with releasing volatiles corresponding to the characteristic decomposition of oxygenated functional groups attached to the amorphous carbon layer from hydrothermal carbons or functionalized CNTs,[44−46] which describes the amorphous/graphitic structural nature of the functionalized CNTs. The observed residual weight is associated with the not-removed catalyst particles after purification of the CNTs.

Surface wettability is a fundamental parameter to evaluate changes in the hydrophilicity/hydrophobic surface nature. In this context, the contact angle was measured by placing a pure water drop of 5 μL on pristine and functionalized CNT films. As shown in Figure 8, the MWCNT-raw film bears a water contact angle of $\theta \approx 121.3°$, which is attributable to the lack or lower number of oxygenated groups on the surface with respect to glucose-coated CNTs. In contrast, the spontaneous spreading of

https://doi.org/10.1021/acsomega.2c08203
ACS Omega 2023, 8, 11233−11250

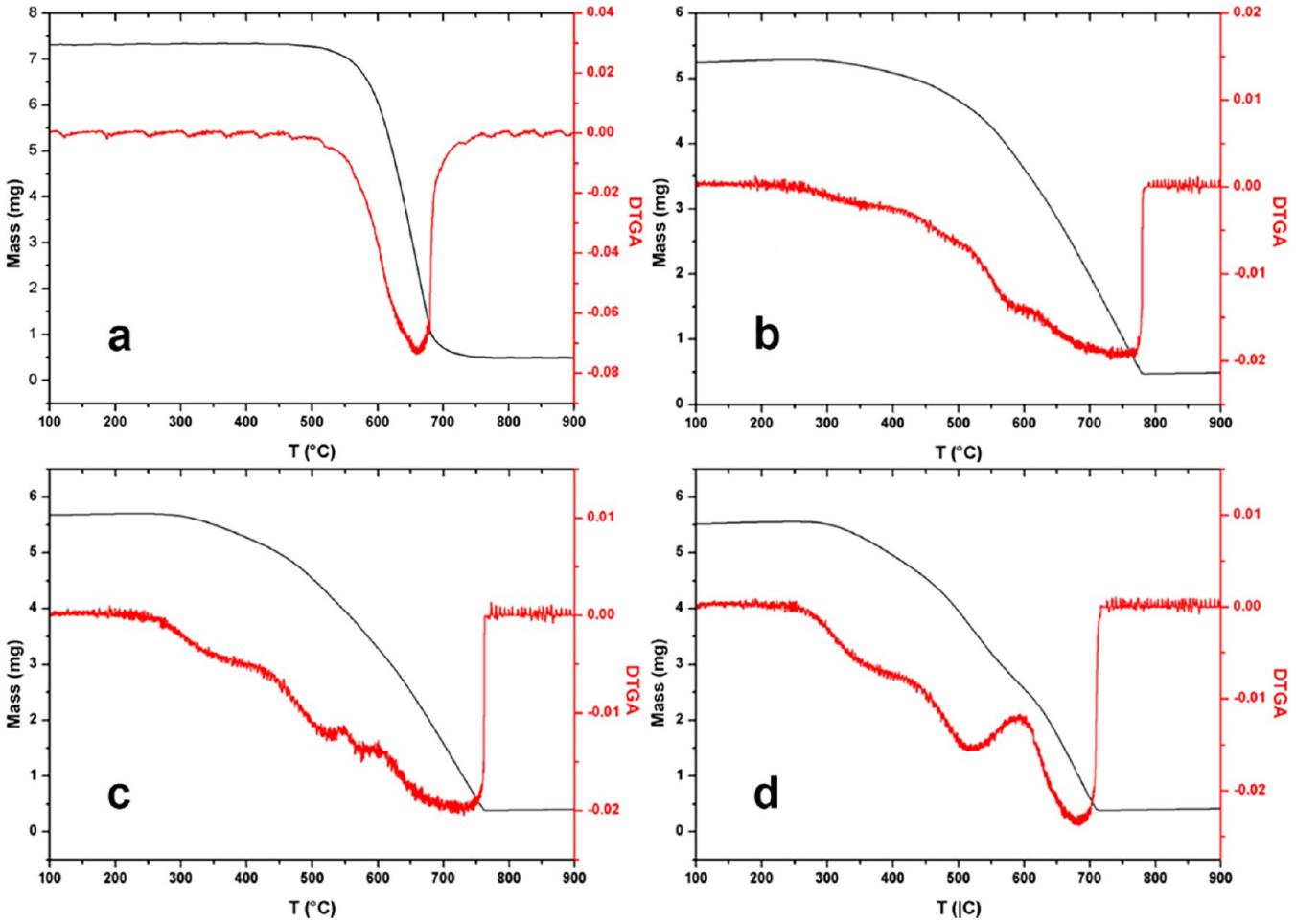

Figure 7. TGA curves of pristine (a) and functionalized MWCNT-COOH-11, -12, and -14 (b−d).

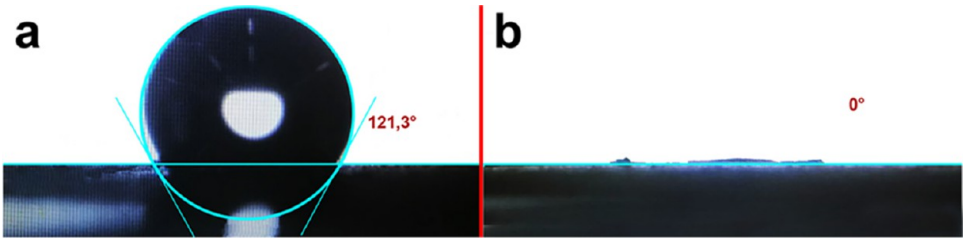

Figure 8. Pictures of drops of pristine MWCNT-raw (a) and functionalized MWCNT-COOH-11, -12, and -14 suspended in water (b), showing the hydrophobic and hydrophilic nature of MWCNT-raw ($\theta \approx 121.3°$) and functionalized MWCNT-COOH-11($\theta \approx 0°$), respectively.

the water drop after 1−2 s is illustrated on functionalized CNTs (-11, -12, and -14). The incorporation of such oxygenated groups on the carbon amorphous layer leads to an improvement of the hydrophilicity of the functionalized CNTs as a function of the increased amount of glucose concentration, and it can be easily dispersed in water vs the intrinsic hydrophobicity observed for MWCNT-raw (Figure 8).[20]

Adsorption Dye Properties on Pristine and Functionalized CNTs. In a preliminary test probe, we chose four dyes, two cationic and two anionic, with distinctive structural features, including charged dyes, different sizes and shapes, and the presence of functional groups with potential affinity with the functionalities available on the sorbent surface. On the basis of the physicochemical characterization aforementioned, different assays were carried out for determination of the dye removal adsorption capacity for all of the functionalized CNTs, including the pristine CNTs. For such assays, similar dye concentrations and adsorbent doses were collocated in contact during 48 h, and the variation of the concentration in each assay at the equilibrium was determined by UV−visible spectroscopy (Figure 9).

Table 3 lists the dye adsorptive capacity of all of the prepared sorbents at the equilibrium. As anticipated, pristine and functionalized CNTs show adsorption capacity either for cationic or anionic dyes with appreciable differences. An interesting case is provided by the MWCNT-raw, in which cationic dyes are preferentially adsorbed vs anionic dyes for pH < pH_{pzc} (pH work values 5−6 for dye solutions). The equilibrium dye adsorption capacity on the pristine surface shows the following trend MV > MB > AY ≈ MO. These results contradict the conventional behavior expected on positively charged surfaces,[17] where anionic dye adsorption should be

https://doi.org/10.1021/acsomega.2c08203
ACS Omega 2023, 8, 11233−11250

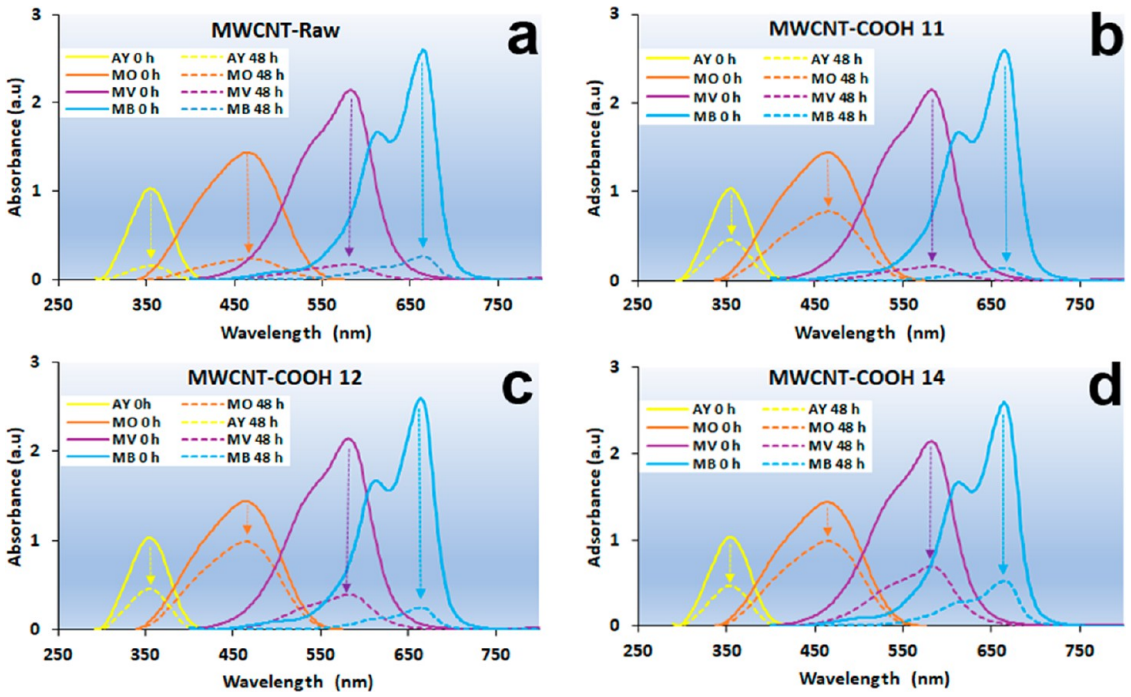

Figure 9. Schematic UV−vis spectra representation of dye adsorption on pristine (a) and functionalized MWCNT-COOH-11, -12, and -14 of MB, MV, MO, and AY (b−d), using dye solutions ($C_o \approx 7 \times 10^{-5}$ mol L^{-1}). Each dye adsorption process was carried out separately, and for comparative analysis was placed on the same graphic. The adsorbent loading was maintained at 0.5 mg mL^{-1} for all cases with a contact time of 48 h at 25 °C.

Table 3. Comparative Adsorption Dye Capacity at the Equilibrium on Pristine and Functionalized MWCNT-COOH-11, -12, and -14, Using Dye Solutions ($C_o \approx 7 \times 10^{-5}$ mol L^{-1})[a]

	adsorption capacity (mg g^{-1})			
adsorbents	MV	MB	MO	AY
MWCNT-raw	52.8	39.1	17.2	17.6
MWCNT-COOH-11	52.2	42.0	6.6	5.1
MWCNT-COOH-12	47.0	40.8	1.1	5.0
MWCNT-COOH-14	41.4	36.7	0.6	4.8

[a]The adsorbent loading was maintained at 0.5 mg mL^{-1} for all cases with a contact time of 48 h at 25 °C.

favorable over cationic dyes. Conventionally, this cationic adsorption affinity explanation is associated with the presence of a higher number of aromatic rings with respect to anionic dyes, leading to the maximization of $\pi\cdots\pi$ interactions. At this point, it is noteworthy that an aspect systematically ignored or improvised in the adsorption process literature is the omission of well-established intermolecular interactions based on the robust and widely exploited homo- and/or heterosynthon toolkit from the Supramolecular Chemistry and Crystal Engineering. For example, an important hierarchical interaction supramolecular interaction like the cation−π interaction[36,37] is not taken into account; when possible, adsorption mechanisms are proposed and might lead to incorrect or speculative interpretations about some adsorption process on materials bearing nitrogen ionizable groups or carbonaceous materials. This interaction contributes to the stabilization of the molecules on such surfaces. Conventionally, authors do not discriminate between these distinct interactions, with cation−π being stronger (5−80 kJ mol^{-1}) than simple $\pi-\pi$ interactions (0-50 kJ mol^{-1}). In such cases, an increment of the cationic dye adsorption capacity to pH < pH_{pzc} is commonly observed.

Adsorption capacity on MWCNT-COOH-11 is similar, showing the following trend MV > MB > MO ≈ AY. The presence of a negative charge on MO and AY dyes induces repulsive anion−π interactions, in contrast to the cation−π interaction, destabilizing the interaction adsorbate/surface with a decrease of ≈3 times the anionic dye adsorptive capacity, which varies from 17.6 to 6.6 and 17.2 to 5.1 mg g^{-1} for MO and AY, respectively. In this case, the presence of oxygenated groups on the surface became negative as indicated by its pH_{pzc} value ($pH_{pzc} \approx 3$).

The dye adsorption capacity for the rest of the functionalized CNTs became lower when the glucose weight ratio is higher with respect to pristine MWCNT-COOH-11, 12, and 14. A gradual diminution for cationic dyes is observed at room temperature (25 °C) from 52.8 to 41.4 and 39.1 to 36.7 mg g^{-1} for MV and MB, respectively. For anionic dyes, the effect is more remarkable, and the dye concentration at equilibrium decreased from 17.2 to 0.6 and 17.6 to 4.8 mg g^{-1} for MO and AY, respectively. This behavior could be associated with the lower surface values found in functionalized MWCNTs, including a possible reduction of the π-surface with respect to pristine CNTs.

Molecular Recognition and Supramolecular Complementarity at Surfaces. To provide new insights into the role of chemical functionalization in adsorption (multivalency and cooperative effects)[21−24] processes using a carbonaceous material as a proof-of-concept demonstration, we evaluated the dye removal capacity as a function of the temperature, selecting pristine and functionalized MWCNT-COOH-11 as adsorbents. This last one contains the highest surface combined with a similar total acid group density. On the other hand, the adsorption isotherm is a well-known effective method to study the adsorption ability of an adsorbent and understand the interactions between the interface adsorbate/adsorbent systems. To illustrate our approach based on the selective removal of

https://doi.org/10.1021/acsomega.2c08203
ACS Omega 2023, 8, 11233−11250

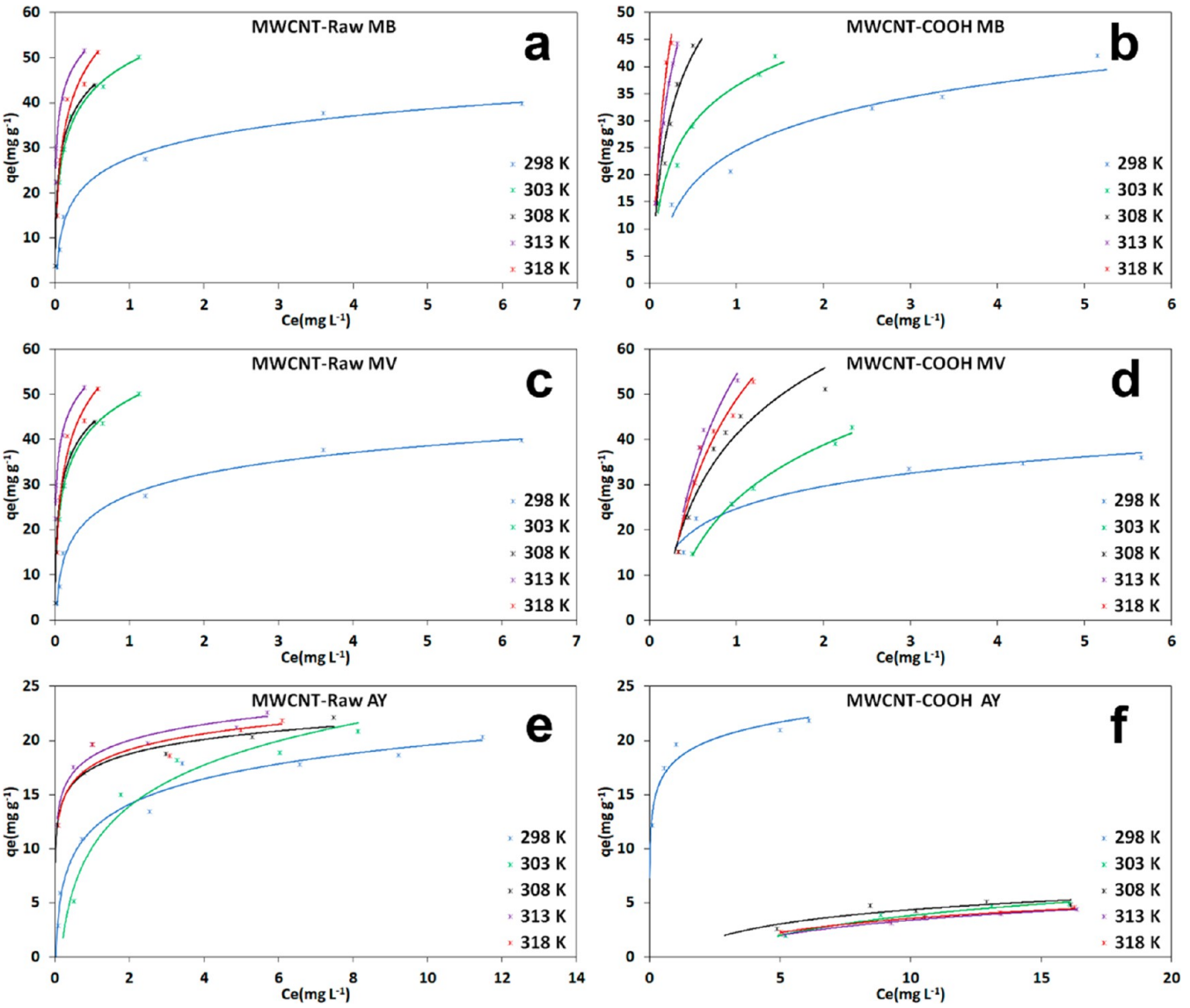

Figure 10. Comparative dye adsorption isotherms for MB (a, b), MV (c, d), and AY (e, f) at different temperatures (298, 303, 308, 313, and 318 K) with pristine and functionalized MWCNT-COOH-11. The adsorbent loading was maintained at 0.5 mg mL^{-1} for both cases, with a contact time of 48 h.

organic dyes directed by surface recognition processes via complementary supramolecular synthons, a set of assays were carried out, including individual and competitive binary adsorption assays (cation/cation, cation/anion, and anion/anion).

Figure 10 shows the variation of the amount of MB, MV, and AY adsorbed at equilibrium on MWCNT-raw and MWCNT-COOH-11 as the function of temperature, with the data fitted by the Langmuir, Freundlich, and Temkin isotherm models (Table 4).[32]

As expected, according to the surface nature, almost all of the isotherms at 298 K exhibit a well-defined plateau, which can be well described by the Langmuir model, which correlates well with the experimental data for both adsorbents. The adsorption capacity on pristine CNTs and functionalized MWCNT-COOH-11 display the following trend MB > MV > AY. These results indicate that the adsorption process on both surfaces is due to monolayer coverage, except for the MV dye on pristine and functionalized CNTs, which is better fitted by the Temkin model (R^2 = 0.988). This result suggests that the adsorption is dominated by ionic interactions between the adsorbent and adsorbate, due to the impossibility of efficiently accommodating this molecule on the curvature of CNTs, in contrast to the rest of the molecules, which can be well-fitted along the axis direction of CNTs.[33] For the cationic dye adsorption isotherms, a temperature dependence was observed. In particular, the removal adsorption capacity on pristine CNTs shows a moderate dependency; the q_{max} at the equilibrium for MB varies from 41.50 to 57.14 mg g^{-1} when the temperature rises from 298 to 318 K. In contrast, MV displays a diminution of the concentration at the equilibrium from 158.73 to 92.59 mg g^{-1}. In the case of anionic dyes, MO and AY show a slight increase of q_{max} from 20.57 to 21.93 mg g^{-1}, respectively. Parameters from the Freundlich model analysis reveal that the adsorption process is favorable for all of the values of $n > 1$.

Adsorption isotherms on MWCNT-COOH-11 are best fitted in Freundlich and Temkin adsorption models with respect to the Langmuir model, and this suggests the presence of some factors

https://doi.org/10.1021/acsomega.2c08203
ACS Omega 2023, 8, 11233−11250

Table 4. Comparative Langmuir, Freundlich, and Temkin Model Parameters for Adsorption of MB, MV, and AY at Different Temperatures (298, 303, 308, 313, and 318 K) with Pristine and Functionalized MWCNT-COOH-11

	Langmuir-MB									
	MWCNT-raw					MWCNT-COOH-11				
T	298 K	303 K	308 K	313 K	318 K	298 K	303 K	308 K	313 K	318 K
q_m (mg g^{-1})	41.50	53.48	47.85	53.19	57.14	47.62	50.25	81.30	103.09	65.80
K_L	2.939	9.842	19.000	62.667	11.667	0.995	2.653	2.510	2.425	2.086
R_L	0.033	0.027	0.022	0.011	0.026	0.036	0.034	0.034	0.034	0.028
R^2	0.996	0.996	0.998	0.997	0.993	0.971	0.934	0.940	0.986	0.988
	Freundlich-MB									
	MWCNT-raw					MWCNT-COOH-11				
T	298 K	303 K	308 K	313 K	318 K	298 K	303 K	308 K	313 K	318 K
n	2.470	3.846	1.952	4.833	2.942	2.783	2.581	1.691	1.352	2.284
K_F	22.7	50.0	81.1	63.8	64.5	22.6	36.3	67.8	107.8	81.5
R^2	0.919	0.960	0.874	0.934	0.841	0.990	0.990	0.987	0.992	0.982
	Temkin-MB									
	MWCNT-raw					MWCNT-COOH-11				
T	298 K	303 K	308 K	313 K	318 K	298 K	303 K	308 K	313 K	318 K
K_T	1.078	1.191	1.174	1.190	1.174	1.093	4.211	1.455	1.643	1.492
b	366.6	278.7	306.3	350.6	330.5	274.9	248.9	149.7	133.1	165.3
R^2	0.991	0.985	0.995	0.969	0.796	0.950	0.968	0.949	0.995	0.981
	Langmuir-MV									
	MWCNT-raw					MWCNT-COOH-11				
T	298 K	303 K	308 K	313 K	318 K	298 K	303 K	308 K	313 K	318 K
q_m (mg g^{-1})	158.73	123.46	312.50	81.97	92.59	39.21	79.37	86.96	238.10	232.56
K_L	0.154	0.496	0.150	0.462	0.830	1.946	0.479	0.833	0.302	0.262
R_L	0.035	0.034	0.035	0.034	0.034	0.032	0.034	0.034	0.034	0.034
R^2	0.354	0.998	0.297	0.994	0.992	0.998	0.983	0.823	0.324	0.284
	Temkin-MV									
	MWCNT-raw					MWCNT-COOH-11				
T	298 K	303 K	308 K	313 K	318 K	298 K	303 K	308 K	313 K	318 K
K_T	1.235	1.491	1.516	1.207	1.410	1.073	1.203	1.402	1.960	1.669
b	121.1	102.7	100.4	144.3	123.1	347.5	144.2	121.5	80.8	94.2
R^2	0.988	0.996	0.990	0.993	0.997	0.945	0.995	0.931	0.963	0.984
	Freundlich-MV									
	MWCNT-raw					MWCNT-COOH-11				
T	298 K	303 K	308 K	313 K	318 K	298 K	303 K	308 K	313 K	318 K
n	1.131	1.365	1.081	1.581	1.646	3.559	1.522	1.448	1.139	1.132
K_F	20.7	40.8	40.8	24.5	41.0	23.5	24.8	39.3	57.1	49.4
R^2	0.915	0.998	0.971	0.989	0.988	0.876	0.982	0.860	0.915	0.922
	Langmuir-AY									
	MWCNT-raw					MWCNT-COOH-11				
T	298 K	303 K	308 K	313 K	318 K	298 K	303 K	308 K	313 K	318 K
q_m (mg g^{-1})	20.57	24.57	22.12	22.47	21.93	21.93	15.94	7.03	9.06	7.96
K_L	1.604	0.664	3.863	6.449	8.291	8.291	0.030	0.130	0.059	0.080
R_L	0.041	0.043	0.038	0.034	0.032	0.032	0.044	0.044	0.044	0.044
R^2	0.994	0.986	0.994	0.997	0.999	0.999	0.526	0.966	0.979	0.993
	Freundlich-AY									
	MWCNT-raw					MWCNT-COOH-11				
T	298 K	303 K	308 K	313 K	318 K	298 K	303 K	308 K	313 K	318 K
n	3.717	2.043	8.496	7.905	7.564	7.564	1.216	2.038	1.516	1.746
K_F	10.6	8.6	17.0	18.1	17.7	17.7	1.8	1.2	1.3	1.0
R^2	0.984	0.871	0.986	0.938	0.904	0.903	0.918	0.939	0.986	0.99

https://doi.org/10.1021/acsomega.2c08203
ACS Omega 2023, 8, 11233−11250

Table 4. continued

	Temkin-AY									
	MWCNT-raw					MWCNT-COOH-11				
T	298 K	303 K	308 K	313 K	318 K	298 K	303 K	308 K	313 K	318 K
K_T	1.015	1.022	1.016	1.012	1.015	1.000	1.002	1.000	1.001	1.000
b	779.7	458.7	1019.2	1536.2	1200.3	2454.0	933.0	971.7	1291.7	1411.6
R^2	0.996	0.941	0.875	0.876	0.936	0.993	0.960	0.010	0.993	0.993

that drive adsorption processes. For example, with the existence of heterogeneous adsorption sites, the adsorption is dominated by ionic interactions between the adsorbent and adsorbate. This mechanism is consistent with the presence of possible charge-assisted hydrogen bond interactions directed by carboxylate−pyridinium or carboxylate−ammonium interactions (Figure 2(II and III)). Such an interaction is in agreement with the pH_{pzc} found for the hydrophilic surface ($pH_{pzc} \approx 3$).

The removal adsorption capacity for dyes over MWCNT-COOH displays some remarkable differences; for example, the adsorption capacity for MB is slightly higher than MV at 298 K. Nevertheless, the cationic dye removal adsorption capacity was significantly enhanced on the hydrophilic surface, but a contrary effect was found for anionic dyes in comparison to MWCNT-raw. Likewise, q_{max} values show higher temperature dependence, and the values for MB and MV show a gradual increase of q_{max} from 47.62 to 103.09 mg g^{-1} at 313 K, followed by a decrease until 65.85 mg g^{-1} at 318 K, whereas MV q_{max} varies from 39.21 to 232.56 mg g^{-1}. This value is higher than the pristine surface. In contrast, AY shows a gradual decrease of ≈2.75 times lower than the pristine surface.

It is important to highlight that this increase in the cationic dye adsorption capacity occurs in an adsorbent with a lower specific area according to the textural analysis (see Table 2). This result shows the importance of the surface chemistry functionality in relation to the adsorption capacity in the case of systems with low porosity.[18,19] This behavior reveals that a large surface area is not necessary for obtaining a higher adsorption capacity than nonporous sorbents.[20,21]

One additional plausible explanation for the increase in the adsorption capacity of cationic dyes onto MWCNT-COOH-11 can be visualized as a better efficient rearrangement of the adsorbate molecules directed by the presence of heterogeneous adsorption sites and assisted by multiple supramolecular interactions. An increase in temperature can facilitate the removal of water molecules that compete for hydrophilic sites and can be occupied by dye molecules (hydrophobic and hydrophilic as shown by the contact angle), and the molecules can be stabilized by interactions of hydrogen of the pyridine−carboxylic acid (Figure 2(II, III)) and pyridine−phenol type (Figure 2(I)), destabilizing or complementing the interactions $\pi-\pi$ and cation$-\pi$ between the dye and the surface. This rearrangement of the molecules as a function of temperature could occur through the formation of a multilayer arrangement as suggested by the adjustment of the Freundlich model. This is also possible by a change in the relative orientation of the molecules in the monolayer from a parallel to a perpendicular or an inclined fashion on the adsorbent surface.

Adsorption Thermodynamics for MB, MV, and AY on MWCNT-Raw and MWCNT-COOH-11. To reveal the mechanism of MB, MV, and AY adsorption on the distinctive surfaces, a set of new experiments were performed at 298, 303, 308, 313, and 318 K. The adsorption thermodynamic parameters were calculated according to the thermodynamic theory using eqs 2 and 3, and the relationships for the $\Delta H°$, $\Delta G°$, and $\Delta S°$ are listed in Table 5.

The adsorption Gibbs free energy ($\Delta G°$) on the pristine surface exhibits large values, being higher toward the adsorption of MB, followed by AY, and finally MV. Similar results are observed on MWCNT-COOH but exhibiting other tendencies for the same dye series for $\Delta G°$ for AY > MV > MB.

This parameter is in good agreement with the results obtained from the isotherm models, demonstrating that all of the adsorption processes on both distinctive surfaces are spontaneous and highly favorable from the thermodynamic point of view. The $\Delta G°$ values for MB exhibit a gradual increase when the temperature is raised, demonstrating that the spontaneous adsorption process on both surfaces is larger at a higher temperature.

According to the classical theory of the adsorption process, the absolute value of the $\Delta G°$ provides a guide for classifying the adsorption-type and depending on these values varies in the range −20 to 0 and −400 to −80 kJ mol^{-1} for physical and chemical adsorption, respectively.[17] In our cases, these values are in the range −54 to −37 kJ mol^{-1}. These larger values suggested that the adsorption processes do not fit the criteria defined for both physisorption and chemisorption. On the basis of the values found, it cannot be classified as simple physical adsorption but neither as pure chemical adsorption.[17] The classical theory based on the adsorption of gases on porous solids, for obvious reasons, does not contemplate robust interactions of a supramolecular nature between the adsorbate/surface, whose interaction energies are greater than weak interactions (van der Walls, dipole−dipole, London dispersion forces, etc.), but weaker than a conventional chemical bond.

In this theory gap, there is a type of adsorption so far not considered, which could be supported by the multivalency provided by the existence of multiple intermolecular interactions of medium hierarchy in terms of energy such as cation$-\pi$ and hydrogen bond synthons. Therefore, a novel classification should be considered to cover this gap in the theory, to avoid incorrect interpretations and its propagation in the literature for an adequate interpretation of the adsorption processes in functionalized systems and supramolecular structures in the future.

An important effect of the functionalization on the CNTs should be reflected in the thermodynamic parameters, in particular, with enthalpic and entropic consequences due to the presence of multiple interaction sites that are covalently bound to the surface, which might lead to increased stability compared to the pristine surface. Introducing functional groups can induce the preorganization of the molecules on the surface through the cooperative effects and/or complementarity interaction of multiple pairs of binding sites between the adsorbate/surface.[22]

A comparative analysis reveals the following results: The enthalpy change ($\Delta H°$) was positive ($\Delta H° > 0$) for the adsorption processes on the pristine CNTs, which suggested

https://doi.org/10.1021/acsomega.2c08203
ACS Omega 2023, 8, 11233−11250

Table 5. Thermodynamic Parameters of the Adsorption of MB, MV, and AY on Pristine and Functionalized MWCNT-COOH-11[a]

T	298 K			303 K			308 K			313 K			318 K		
	MB	MV	AY	MB	MV	AY	MB	MV	AY	MB	MV	AY	MB	MV	AY
MWCNT-Raw															
ΔG^0 (kJ mol^{-1})	−44.05	−37.27	−42.46	−47.83	−38.95	−40.95	−50.31	−38.45	−46.14	−54.23	−42.20	−48.22	−50.65	−42.91	−49.66
ΔH^0 (kJ mol^{-1})	18.97	5.96	8.00												
ΔS^0 (J K^{-1} mol^{-1})	80.40	35.10	44.00												
R^2	0.988	0.957	0.992												
MWCNT-COOH-11															
ΔG^0 (kJ mol^{-1})	−41.36	−43.56	−46.54	−44.53	−40.75	−33.15	−45.12	−42.84	−37.45	−45.76	−40.90	−36.00	−46.10	−41.17	−37.38
ΔH^0 (kJ mol^{-1})	−1.45	−10.15	−23.00												
ΔS^0 (J K^{-1} mol^{-1})	12.9	−16.44	−60.00												
R^2	0.892	0.950	0.843												

[a]The adsorbent loading was maintained at 0.5 mg mL^{-1} for all cases with a contact time of 48 h.

that the adsorptions were endothermic processes, and consistent with the fact that the adsorption capacity increased with the increase of temperature in the case of MB and AY. In contrast, the enthalpy change was negative ($\Delta H^\circ < 0$) for all of the adsorption processes on MWCNT-COOH-11, which suggested that the adsorptions were exothermic processes, being the lower value found for AY, which was consistent with a decrease of the adsorption capacity with the increase of temperature. This difference is associated with the higher or lower affinity of the adsorbed water molecules on the distinctive surfaces (see Figure 8). As a previous step to the adsorption of the dye molecules, water molecules must first be released from the surface before the adsorption of the organic molecules.

A more sensitive parameter to functionality is represented by the changes in the entropy values (ΔS°) between the systems, finding a strong decrease in entropy when passing from the adsorption on the pristine to the MWCNT-COOH-11. For the case of MB, a decrease of ≈67 J K^{-1} mol^{-1} is observed, which reveals the possibility of some structural changes or rearrangements in the MB/MWCNT-COOH-11 adsorption system, at the liquid/solid interface vs the MB adsorption interface/MWCNT-raw.

In the case of MV and AY, their ΔS° values were more negative, which shows a higher order in their adsorption on the surface of MWCNT-COOH-11 vs the surface of MWCNT-raw, which represents a decrease in ΔS° of ≈52 and 104 J K^{-1} mol^{-1}, for MV and AY, respectively. In all of the dye/MWCNT-COOH-11 systems, these values suggested an increase of the organization of the molecules in the liquid/solid interface as expected, as a consequence of the decrease in the degrees of freedom of these molecules due to the multivalency character that offers the functionalized surface through the establishment of multiple interactions, both hydrophobic and hydrogen bonds, that lead to a possible cooperative effect.

Selective Adsorption Studies of Binary Mixtures on Pristine and Functionalized MWCNT-COOH-11. To gain further insights to help understand, the parameters involved in the adsorption processes were provided for a new set of adsorption assays. Studies on the selective removal of dyes from binary mixtures in solution were evaluated. Thus, we performed two types of competitive sorption experiments employing both adsorbents. In the first place, selective adsorption assays of a mixture of dyes were chosen on the basis of previous affinity adsorbate/surface analysis. Second, mixtures of cationic dyes were also studied to evaluate their ability and efficiency and their distinctive donor/acceptor capacities; for example, molecules with multivalent available acceptor/donor sites are expected to be stronger competitors than molecules with a lower acceptor/donor capacity. The selective adsorption of the following binary mixtures was tested: MB/MV, MB/MO, MB/AY, MO/AY, MV/MO, and MV/AY. Color changes were visible to the naked eye, and quantification was performed by UV−vis spectroscopy (Figure 11). For the assays bearing cationic dye mixtures, concomitant adsorption of the components was observed for all of the mixtures either on pristine or MWCNT-COOH-11. In both cases MB, MV are adsorbed in a lower percentage than MV and MB by being separated on both surfaces, with the following relative percentage values at equilibrium: MB 68.5% and MV 73.0%; MB 72.9% and MV 88.0%, on pristine and MWCNT-COOH-11, respectively. Apparently, this difference is attributed to the inefficient stacking of two molecules with different sizes on the monolayer, generating empty spaces that are not well-fitted to accommodate these molecules. Thus, the resulting color

https://doi.org/10.1021/acsomega.2c08203
ACS Omega 2023, 8, 11233−11250

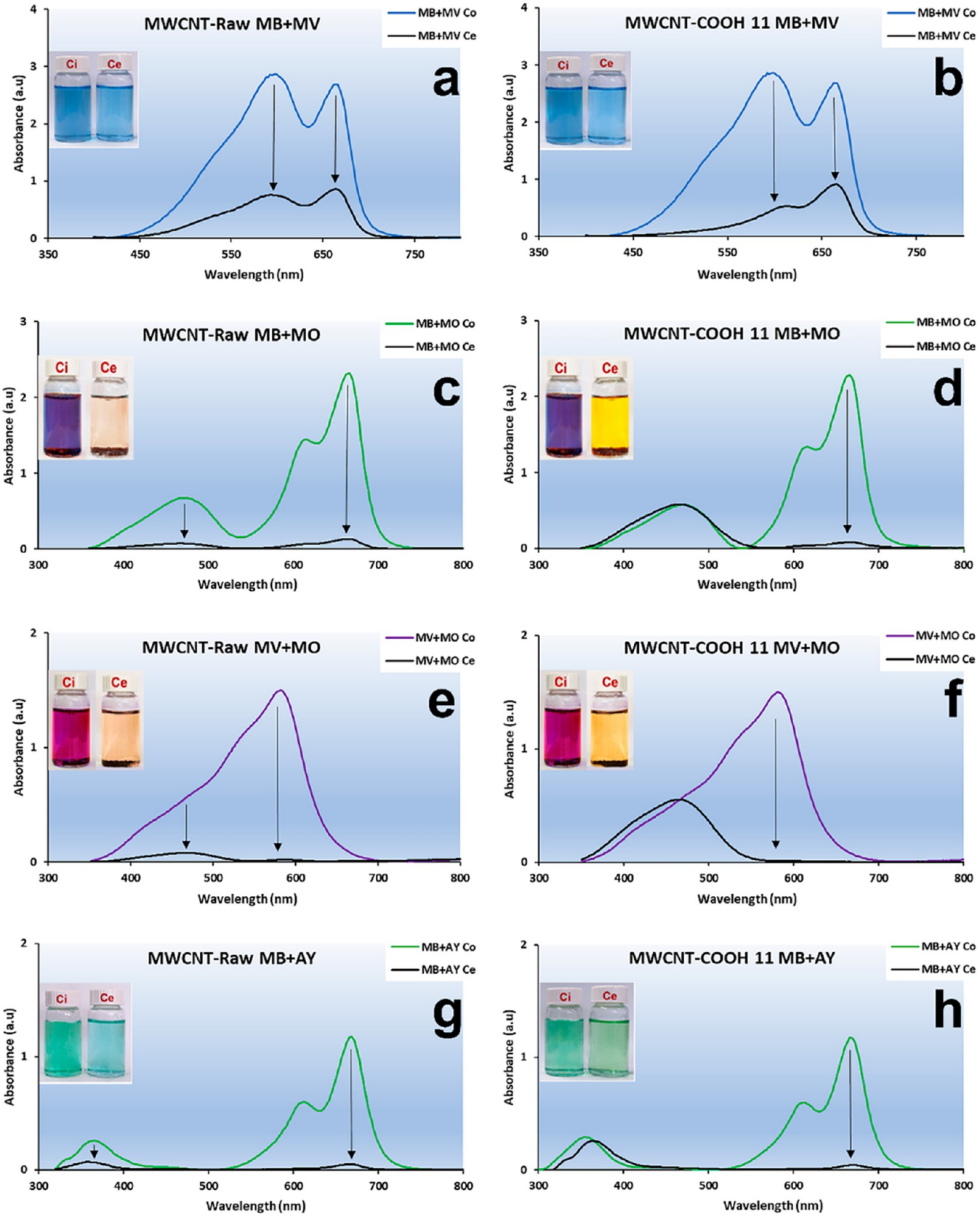

Figure 11. continued

https://doi.org/10.1021/acsomega.2c08203
ACS Omega 2023, 8, 11233−11250

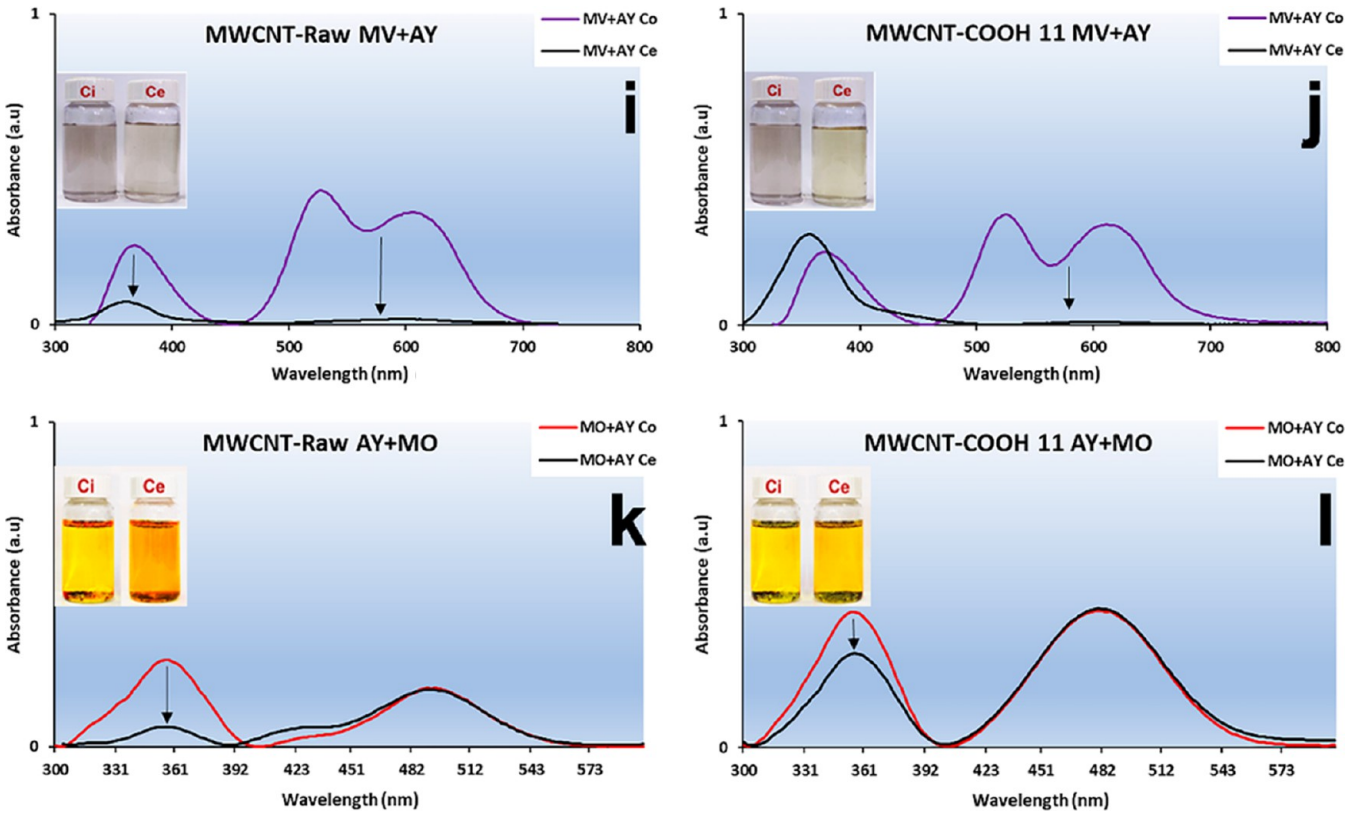

Figure 11. Comparative UV−vis absorption spectra for evaluating the selective adsorption capability of pristine and functionalized MWCNT-COOH-1 from mixed dyes: top/bottom MB/MV (a, b), MB/MO (c, d), MV/MO (e, f), MB/AY (g, h), MV/AY (i, j), and AY/MO (k, l), using solutions with a similar concentration ($C_o \approx 7 \times 10^{-5}$ mol L^{-1}) and similar solution volume (10 mL) for each dye. The sorbent loading was maintained at 0.5 mg mL^{-1} for all of the cases, with a contact time of 48 h. Insets: photographic images showing the characteristic color of the solutions before (left) and after (right) dye adsorption at equilibrium.

from the combination of the dyes and the adsorbent revealed a gradual decrease of the original coloration, indicating the simultaneous adsorption of both dyes. On the other hand, when a cationic/anionic mixture was used a contrary effect was observed on the pristine surface; either cations or anions are adsorbed in a higher percentage than each component by being separated on both sorbents, with relative percentage values at equilibrium AM + MO: AM 94.9% and 89.5%; AM + AY: AM 96.75%, AY: 75.5%, VM + MO: VM 98.23%, MO: 91.0%; VM + AY: VM: 95.7%, AY:29.6%, whereas the adsorption on the functionalized surface is completely different, in these cases the preferential and induced selective adsorption is MB or MV over MO and AY, respectively. In such solutions, the color of the initial solution gradually changed and revealed the characteristic color associated with the pure anionic after addition of MWCNT-COOH-11, such changes indicate that cationic MB and MV were selectively removed from the mixture, whereas the absorption band of the anion dye in the mixed solution remained essentially unchanged. A similar effect was also observed for the anionic dye mixtures MO/AY dyes on MWCNT-raw and MWCNT-COOH-11. To our surprise, AY is adsorbed selectively over MO (Figure 11(k, l))

It is noteworthy that anionic dyes showed lower affinity than cationic dyes, independent of whether the surface is hydrophobic or hydrophilic, even when the dye molecules display potential chemical groups with the ability to interact with the distinctive surfaces either via hydrogen bonding interactions or $\pi-\pi$ interactions. The adsorption of the same anionic mixture on MWCNT-COOH-11 exhibits a similar trend but with an adsorption capacity lower than found for the pristine surface; anionic dyes are not adsorbed significantly on hydrophilic CNTs. Competitive assays from cationic/anionic and anion/anion mixtures revealed interesting results, confirming that the molecules with a higher number of donor/acceptor sites show a remarkably larger affinity for the hydrophilic surface than the molecules with a lower donor/acceptor capacity.[20] Likewise, interaction of anion$-\pi$ suggested that it can be used for selective removal and separation of anions on hydrophobic or hydrophilic surfaces,[47] being more efficient on hydrophobic surfaces. A comparative analysis of the dye azo molecules MO and AY display similar structures; although AY contains $-OH$, $-NO_2$, and $-COO^-$ groups, the molecule can adopt a flat configuration, allowing a higher affinity on the surface-π than $-N(CH_3)_2$ and $-SO_3^-$ groups bearing in MO molecules.

Taking into account such structural features provided by the functionalization with oxygenated groups and assuming that the capacity adsorption is effectively directed by surface recognition, we expected that the trend in the adsorptive capacity would be larger in the dye molecules that have a higher acceptor/donor capacity.[21] Thus, additional competitive assays were carried out to demonstrate this approach.

Further evidence was provided to validate the anticipated selective affinity of cationic and anionic dyes based on multivalent donor/acceptor interactions for both surfaces. After single or binary component adsorption assays at the equilibrium, saturated samples with each cationic or anionic dye mixture on pristine and hydrophilic CNTs were centrifuged and liquid discarded (MB-MV/MWCNT-raw, MV-MO/MWCNT-

https://doi.org/10.1021/acsomega.2c08203
ACS Omega 2023, 8, 11233−11250

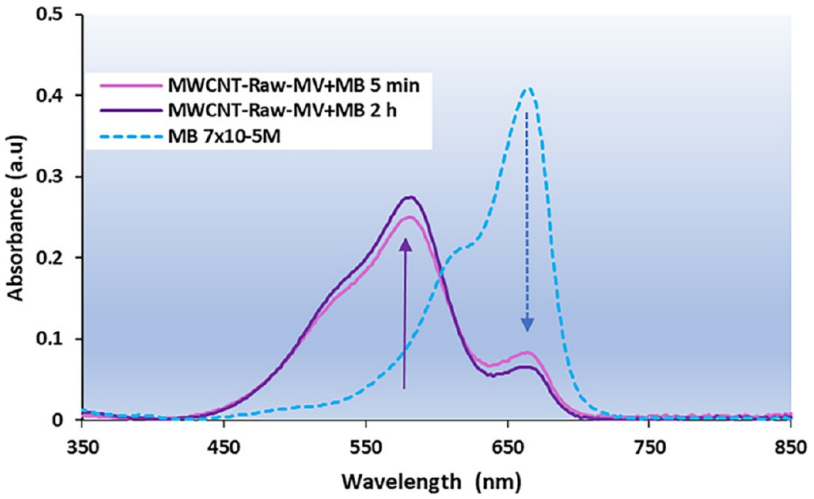

Figure 12. Representative UV−vis absorption spectra of competition cationic-exchange adsorption processes from saturated MV/MWCNT-raw in the presence of 10 mL of MB ($C_o \approx 7 \times 10^{-5}$ mol L^{-1} at 298 K).

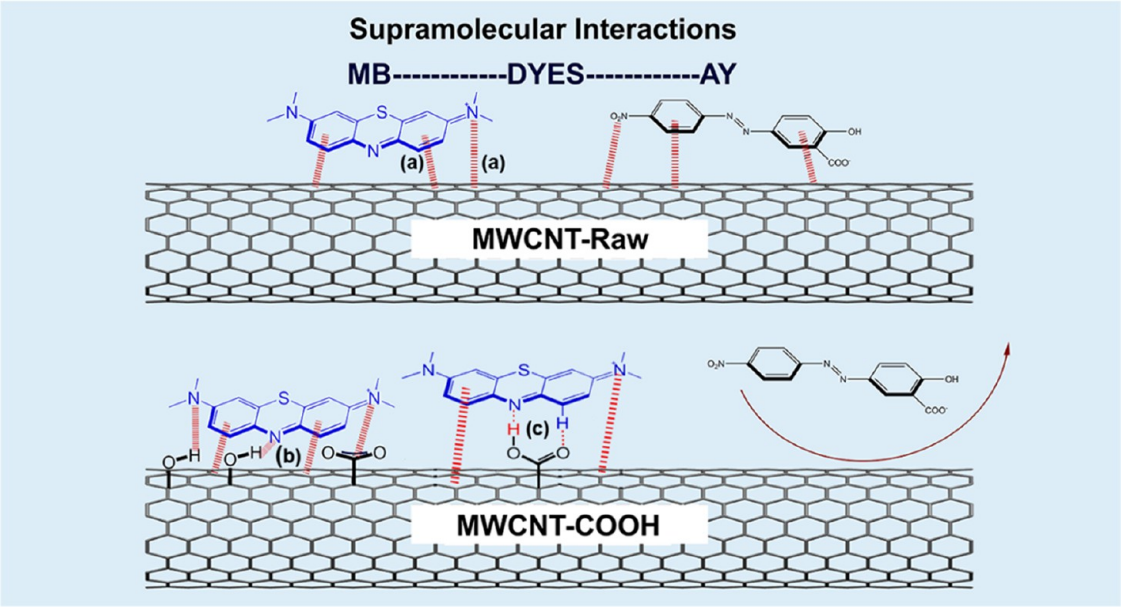

Figure 13. Schematic representation of possible supramolecular interaction modes between pristine and functionalized CNTs and MB and AY dyes, showing cation−π and $\pi\cdots\pi$ interactions on the pristine surface and multivalent interactions on the hydrophilic CNT surface (a) cation−π and $\pi\cdots\pi$; (b) O−H···pyridine; and (c) heterosynthon carboxylic acid−pyridine.

raw, MV/MWCNT-raw). These dye-saturated solids were soaked with a fresh solution of MB (10 mL at 6×10^{-5} mol L^{-1}). Interesting competitive cationic or anionic exchange adsorption processes were observed with respect to time. The cation in solution with the highest multivalent capacity has the ability to induce a partial or total exchange of the adsorbed dye from the surface. UV−vis spectra show that the intensity of MB in solution decreases with time. Simultaneously, the solution gradually exhibits an increase of the characteristic color of the dye released: MV or MO in each case. Figure 12 shows the representative exchange of MV by the MB dye in the MB-MV/MWCNT-raw and MV/MWCNT-raw systems.

At the present stage, some insights can be drawn to explain the results of the different adsorption assays: (a) The aforementioned experimental findings indicate that chemical modification by switching from a hydrophobic surface to hydrophilic MWCNT-COOH-11 provides interesting adsorption properties. This superficial modification leads to remarkable induced dye removal selectivity, depending on the charge, multivalency capacity, and temperature, which can be highly selective and tunable for cationic dyes, allowing a higher affinity on the surface by simply modifying the supramolecular domain and its ability to interact via complementary interactions based on well-recognized supramolecular synthons (Figure 2). (b) Such selectivity strongly suggests the existence of a real positive synergistic effect as a direct consequence of the cooperative matching of multiple interactions between the adsorbate/MWCNT-COOH-11. In these surfaces, cation−π and anion−π interactions[42] might also play a significant role in the selectivity of the adsorption process, interactions that commonly are not taking account in molecular dye adsorption. (c) Likewise, a rare example of a negative cooperative effect could be visualized with the adsorption of anionic dyes on the hydrophilic surface, where an anion−π repulsive interaction is stronger than the

https://doi.org/10.1021/acsomega.2c08203
ACS Omega 2023, 8, 11233−11250

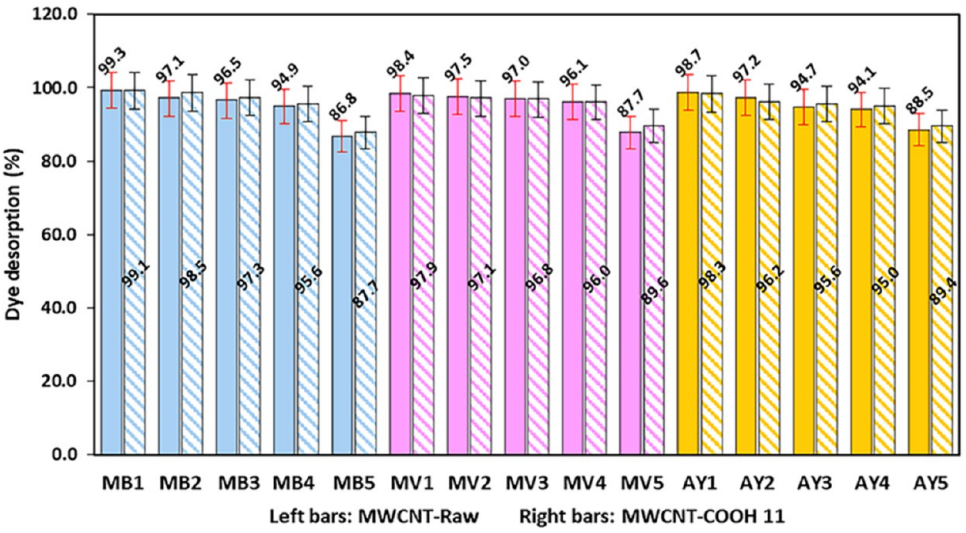

Figure 14. Recycling studies of MB, MV, and AY on the pristine and functionalized CNTs over five cycles (0.5 mg mL^{-1} at 298 K).

stabilization found for a cationic dye on the same surface via attractive cation−π and multivalent interactions. (d) On the other hand, the adsorption process on pristine CNTs is dominated mainly by $\pi-\pi$ and electrostatic interactions (cation−π and anion−π). Thus, several possibilities on the potential use of supramolecular interactions are outlined for the selective removal and separation of cations and anions on different surfaces (Figure 13).

Regenerability of Pristine and Functionalized CNTs. The regenerability of both adsorbents was evaluated. A mixture of methanol/water in a 1:1 V/V ratio was used to remove MB, MV, and AY from saturated solids, dye/MWCNT-raw and dye/MWCNT-COOH-11. Simple washing for the removal of cationic dyes was effective, leading to dye release up to initial adsorbed values according to UV−vis spectra, resulting in contact showing that the absorbance intensity of MB, MV, and AY increase with time (Figure 14). There were no obvious changes in the adsorption efficiency of the regenerated pristine and functionalized absorbents, at least after four times, preserving the adsorption removal capacity nearly to 95% of fresh adsorbents. Finally, a higher loss adsorption capacity is observed after five adsorption−desorption cycles. The decrease in the desorption percentages could be attributed to the sequential loss of the adsorbent mass during the filtering and washing cycles. These results reveal that both adsorbents could be used repeatedly in multiple rounds of adsorption−desorption without significantly decreasing their adsorption performance. The effect of the cyclic regeneration is shown in Figure 14. This ability is highly desirable in wastewater treatment and is closely related to the lack of internal porosity.

MATERIALS AND METHODS

Chemicals. All reagents and solvents were purchased from commercial sources and were used without further purification.

Carbon Nanotube (CNT) Preparation. Multiwalled-carbon nanotubes (MWCNTs) were prepared by catalytic chemical vapor deposition (CCVD), using acetylene as the carbon source and Fe−Co/CaO as the catalyst precursor, and then purified under acidic conditions, as reported in the literature.[39] Typically, a quartz crucible containing 50 mg of the FeCo/CaO catalyst was placed inside a quartz tube, filled with argon, and heated to 750 °C, and then acetylene was introduced as a carbon source maintaining an Ar/acetylene ratio of 20:180 sccm. After 15 min of reaction time, the acetylene valve was closed and the reactor was cooled down until a temperature below 50 °C was reached and the carbonaceous material was collected for further purification. CNT purification was carried out by refluxing the CNTs in a 5% HCL solution for 3 h, to remove the metals and the support from the catalyst. Then, the purified CNTs were rinsed with distilled water, filtered, and dried at 120 °C for about 6 h.

Hydrothermal Functionalization and Characterization of CNTs. Briefly, 100 mg of CNTs was added to glucose aqueous solutions (10 mL) at fixed-weight CNTs/glucose ratios of 1:1, 1:2, and 1:4, inside a PTFE-lined stainless-steel reactor. The mixture was sonicated for 3 min and then sealed and labeled MWCNT-COOH-11, MWCNT-COOH-12, and MWCNT-COOH-14, respectively. The hydrothermal reactor was placed in a Felisa programmable oven and reacted at 180 °C for 24 h. When the reactor was cooled, the remaining overpressure was released, the reactor was opened, and the solid residue in the reactor was filtered and washed several times with distilled water, and finally dried in air at 60 °C for 24 h.

Fourier-transform infrared (FT-IR) spectroscopy studies were carried out with a Thermo Scientific Nicolet IS10 using KBr pellets. The surface morphologies of CNTs and functionalized CNTs were characterized by an FEI QUANTA 250 FEG scanning electron microscope. Structural analysis at the nanometer scale was performed using a high-resolution electron microscope (HRTEM) JEOL JEM-2100. Surface area determinations by nitrogen adsorption using the Brunauer−Emmett−Teller (BET) method were carried out on a Micromeritics ASAP 2010 instrument. The wettability characterization of the CNTs was performed by a Dataphysics OCA-20 contact angle measuring device with SCA20 software. An automated microsyringe system released a liquid droplet having a volume of 5 μL on the substrate surface. The shape of the droplet on the films was recorded using a coupled digital camera. All of the measurements were performed under ambient conditions (i.e., a temperature of ∼25 °C) and were completed within a few seconds to minimize the effect of evaporation on the contact angle measurements. The standard deviation in the contact angle measurement is ±2°. The point of zero charge (pH_{pzc}) and

https://doi.org/10.1021/acsomega.2c08203
ACS Omega 2023, 8, 11233−11250

the surface acidic group determination of the adsorbents were determined according to the literature.[40,41]

Boehm Titration. The oxygenated surface groups were determined according to the method of Boehm; 200 mg of the CNT sample was placed in 50 mL of the following: 0.05 N sodium hydroxide and hydrochloric acid. The vials were sealed and shaken for 24 h, and then 5 mL of each filtrate was pipetted, and the excess of the base and acid was titrated with HCl and NaOH, respectively. The number of acidic sites of various types was calculated under the assumption that NaOH neutralizes carboxyl, phenolic, and lactonic groups; the number of surface basic sites was calculated from the amount of hydrochloric acid that reacted with carbon.

The points of zero charge (pH_{pzc}) of the adsorbents were determined by adding 50 mL of 0.050 mol L^{-1} NaCl to several Erlenmeyer flasks. A range of initial pH (pH_i) values of the NaCl solutions were adjusted from 2.0 to 10.0 by adding either 0.1 mol L^{-1} of HCl or NaOH. The pH_i values of the solutions were then accurately noted and 50.0 mg of MWCNT-raw and functionalized MWCNT-COOH was added to each flask, which was securely capped immediately. The suspensions were shaken in a shaker at 25 °C and allowed to equilibrate for 48 h. The suspensions were then centrifuged at 4000 rpm for 10 min and the final pH (pH_f) values of the supernatant liquid were recorded. The value of pH_{pzc} is the point where the curve of pH ($pH_f - pH_i$) vs pH_i crosses the line equal to zero.

Organic Dye Adsorption and Desorption. The adsorption experiments were carried out in triplicate at room temperature (25 °C) in a batch system. Prior to each adsorption assay, the sorbents were kept in an oven at 60 °C for 48 h for complete removal of moisture. Batches of the powdered adsorbent (10 mg each) were added to 20 mL of aqueous solutions of methylene blue (MB), methyl violet (MV), methyl orange (MO), and alizarin yellow (AY) ($C_0 \approx 7 \times 10^{-5}$ mol L^{-1}), in glass vials and sonicated for 2 min. After the adsorption equilibrium was reached, the aliquots were removed to determine the remaining concentrations of dyes by UV−vis spectrophotometry. Dye adsorption experiments were also accomplished to obtain isotherms at various temperatures [(25−45) °C]. The amount of dye adsorbed by the adsorbent, q_e (mg g^{-1}), was calculated by the following mass balance relationship

$$q_e = (C_0 - C_e)V/W \quad (1)$$

where C_0 and C_e are the initial and equilibrium dye concentrations in solution, respectively (mg L^{-1}), V is the volume of the solution (L), and W is the mass (g) of the adsorbent used. To discover the adsorption capacity of CNTs, the experimental data were analyzed by the Langmuir, Freundlich, and Temkin isotherm equations. The thermodynamic parameters, free energy change (ΔG°), enthalpy change (ΔH°), and entropy change (ΔS°) for the adsorption of the dye onto CNTs were calculated using the following equations

$$\Delta G^\circ = -RT \ln K_0 \quad (2)$$

$$\Delta S^\circ = \Delta H^\circ - \Delta G^\circ T \quad (3)$$

where K_0 is the thermodynamic equilibrium constant. Values of K_0 are obtained by plotting a straight line of (q_e/C_e) vs q_e. The intercept of the vertical axis gives the K_0 value. The ΔH° is determined from the slope of the regression line after plotting ln K_0 against the reciprocal of the absolute temperature, $1/T$. R is the universal gas constant (8.314 kJ mol^{-1} K^{-1}), and T is the temperature (K).

Selective dye adsorption experiments from binary mixtures were carried out. Typically, a fresh CNT sample (10 mg) was put into the mixed dye solutions (20 mL). The mixed dye solutions were prepared from equal volumes of the two corresponding solutions with the same concentrations (7×10^{-5} mol L^{-1}). UV−vis spectra were recorded to determine the selective adsorption ability of CNTs at given time intervals.

The stock solution of each dye under study was the first set up. The 5×10^{-4} mol L^{-1} stock solutions of dyes were prepared by dissolving each dye powder into 1000 mL of distillate water. Then, the stock solution for these dyes was diluted based on the required initial concentration between 5.0×10^{-6} to 7×10^{-5} mol L^{-1} for adsorption studies. The standard calibration curve measurement was done by measuring the absorbance by UV−visible spectroscopy of each diluted solution at the wavelength that corresponds to the maximum absorbance of each dye. The standard calibration curve measurement was repeated until the obtained regression coefficient, R^2 was nearest to 1. The concentration of each dye in the binary mixture was determined using a standard calibration curve, constructed by mixing two selected pairs of dye solutions while maintaining the same concentration in the final solution. Then, the absorbance by UV−visible spectroscopy of each solution at the wavelength that corresponds to the maximum absorbance of each dye in the mixture was measured. The final concentration of each dye in solution was also measured by calculating the area under the curve. All of the results were found satisfactory and reproducible according to the regression coefficient, R^2 values.

To check the reuse of the CNTs as the adsorbent for the adsorption of the selected dyes, first, CNTs (10 mg) were saturated with 20 mL of dye solutions ($C_o \sim 7 \times 10^{-5}$ mol L^{-1}). After 48 h, the adsorbent was separated by centrifugation, and the liquid was discarded. The solid obtained was added to 20 mL of ethanol and saturated aqueous NaCl solution. After washing with distilled water, the adsorbent was used for the additional cyclic adsorption−desorption process. The dye release was monitored by UV−vis spectroscopy.

CONCLUSIONS

In summary, in this contribution, we have described the obtention of novel multivalent hydrophilic MWCNT-COOH via hydrothermal glucose-coated carbonization. We have demonstrated the potential of the resulting "supramolecular adsorbents" as inexpensive and easily regenerable materials for the selective removal and separation of cationic and anionic dyes from aqueous solution induced by tuning supramolecular surface recognition via single or multiple supramolecular synthons. On the basis of our comparative adsorption studies of different dyes using cationic or anionic molecules on functionalized and MWCNT-raw together with competitive preferential adsorption tests, we have attempted to give new insights into substrate/adsorbent interactions of how reliable hierarchical supramolecular interactions work on distinctive surfaces. Well-known supramolecular concepts such as multivalency, homo−heterosynthons, and cooperative effects (positive or negative) on the adsorption process should be positioned as a well-established habit in the scientific language to provide a correct description and full interpretation of different adsorption processes, depending on the surface chemistry and matching with multivalent molecules. In particular, the adsorption process on novel materials is based

https://doi.org/10.1021/acsomega.2c08203
ACS Omega 2023, 8, 11233−11250

on supramolecular-self-assembly such as metal−organic frameworks, inorganic−organic hybrid materials, covalent organic frameworks among others.[15,48−53] On the other hand, this approach provides an interesting low-cost and green alternative preparation of novel functionalized adsorbents as a potential substitute for activated carbon as the most commonly used standard adsorbent.

We expect that the present findings open an avenue of opportunities for the rational design of tailor-made nanoadsorbents based on well-known molecular recognition processes to direct the selective adsorption and/or separation of complex molecule mixtures for chromatography applications, including multistep adsorption/desorption processes induced by tunable surface and/or supramolecular interactions. Further work on the potential use of other pristine and functionalized surface shape-dependent adsorbents is currently being explored on diverse environmental and chemical untreated sewage by our research group.

AUTHOR INFORMATION

Corresponding Author

Alexander Briceño − *Instituto Venezolano de Investigaciones Científicas (IVIC), Centro de Química, Laboratorio de Síntesis y Caracterización de Nuevos Materiales, Caracas 1020-A, Venezuela;* orcid.org/0000-0001-9798-9406; Email: aobriceno@gmail.com

Author

José Arévalo-Fester − *Instituto Zuliano de Investigaciones Tecnológicas (INZIT), Estado Zulia 4001, Venezuela; Instituto Venezolano de Investigaciones Científicas (IVIC), Centro de Química, Laboratorio de Síntesis y Caracterización de Nuevos Materiales, Caracas 1020-A, Venezuela*

Complete contact information is available at: https://pubs.acs.org/10.1021/acsomega.2c08203

Notes

The authors declare no competing financial interest.

ACKNOWLEDGMENTS

The authors thank FONACIT for financial support through Project PEI-2013002269. Also, they thank T. González, Y. Díaz and E. Cañizales (Intevep-PDVSA) for technical assistance.

REFERENCES

(1) Lehn, J. M. *Supramolecular Chemistry: Concepts and Perspestives*; VCH: Weinheim, Germany, 1995; pp 1−206.

(2) Amabilino, D. Surfaces for Supramolecular Systems. In *Monographs in Supramolecular Chemistry*; RSC Publishing: Cambridge, U.K., 2016; Vol. *19*, pp 1−47.

(3) Mali, K. S.; Pearce, N.; De Feyter, S.; Champness, N. R. Frontiers of supramolecular chemistry at solid surfaces. *Chem. Soc. Rev.* **2017**, *46*, 2520−2542.

(4) Ariga, K.; Ito, H.; Hill, J. P.; Tsukube, H. Molecular Recognition: From Solution Science to Nano/Materials Technology. *Chem. Soc. Rev.* **2012**, *41*, 5800−5835.

(5) Ma, J.; Zhang, Y.; Zhao, B.; Jia, Q. Supramolecular adsorbents in extraction and separation techniques - A review. *Anal. Chim. Acta* **2020**, *1122*, 97−113.

(6) Homaeigohar, S. The Nanosized Dye Adsorbents for Water Treatment. *Nanomaterials* **2020**, *10*, No. 295.

(7) Ahmad, A.; Mohd-Setapar, S. H.; Chuong, C. S.; Khatoon, A.; Wani, W. A.; Kumar, R.; Rafatullah, M. Recent Advances in New Generation Dye Removal Technologies: Novel Search of Approaches to Reprocess Waste Water. *RSC Adv.* **2015**, *5*, 30801−30818.

(8) Radovic, L. R.; Moreno-Castilla, C.; Rivera-Utrilla, J. *Chemistry and Physics of Carbon*; Radovic, L. R., Ed.; Marcel Dekker: New York, 2001; Vol. *27*, pp 227−405.

(9) Li, L.; Quinlivan, P. A.; Knappe, D. R. U. Effects of Activated Carbon Surface Chemistry and Pore Structure on the Adsorption of Organic Contaminants from Aqueous Solution. *Carbon* **2002**, *40*, 2085−2100.

(10) Chang, B.; Guan, D.; Tian, Y.; Yang, Z.; Dong, X. Convenient Synthesis of Porous Carbon Nanospheres with Tunable Pore Structure and Excellent Adsorption Capacity. *J. Hazard. Mater.* **2013**, *262*, 256−264.

(11) Yilmaz, M. D.; Huskens, J. Orthogonal supramolecular interaction motifs for functional monolayer architectures. *Soft Matter* **2012**, *8*, 11768−11780.

(12) Olubummo, A.; Schulz, M.; Schops, R.; Kressler, J.; Binder, W. H. Phase Changes in Mixed Lipid/Polymer Membranes by Multivalent Nanoparticle Recognition. *Langmuir* **2014**, *30*, 259−267.

(13) Pérez-García, L.; Amabilino, D. B. Spontaneous resolution under supramolecular control. *Chem. Soc. Rev.* **2002**, *31*, 342−356.

(14) Mali, K. S.; Pearce, N.; De Feyter, S.; Champness, N. R. Frontiers of supramolecular chemistry at solid surfaces. *Chem. Soc. Rev.* **2017**, *46*, 2520−2542.

(15) Yusuf, M.; Elfghi, F. M.; Zaidi, S. A.; Abdullah, E. C.; Khan, M. A. Applications of Graphene and its Derivatives as an Adsorbent for Heavy Metals and Dyes Removal: A Systematic and Comprehensive Overview. *RSC Adv.* **2015**, *5*, 50392−50420.

(16) Yang, J.-M.; Zhang, R.-Z.; Liu, Y.-Y. Superior adsorptive removal of anionic dyes by MIL-101 analogues: the effect of free carboxylic acid groups in the pore channels. *CrystEngComm* **2019**, *21*, 5824−5833.

(17) Li, C.; Xiong, Z.; Zhang, J.; Wu, C. The Strengthening Role of the Amino Group in Metal-Organic Framework MIL-53 (Al) for Methylene Blue and Malachite Green Dye Adsorption. *J. Chem. Eng. Data* **2015**, *60*, 3414−3422.

(18) Gao, C.-Y.; Yang, Y.; Ai, J.; Tian, H.-R.; Li, L.-J.; Yang, W.; Dang, S.; Sun, Z.-M. A Multifunctional Mn^{II} Phosphonate for Rapid Separation of Methyl Orange and Electron-Transfer Photochromism. *Chem. - Eur. J.* **2016**, *22*, 11652−11659.

(19) Jia, Z.; Li, Z.; Li, S.; Li, Y.; Zhu, R. Adsorption Performance and Mechanism of Methylene Blue on Chemically Activated Carbon Spheres Derived from Hydrothermally-Prepared Poly(Vinyl Alcohol) Microspheres. *J. Mol. Liq.* **2016**, *220*, 56−62.

(20) Trujillo, P.; González, T.; Brito, J. L.; Briceño, A. Surface Recognition Directed Selective Removal of Dyes from Aqueous Solution on Hydrophilic Functionalized Petroleum Coke Sorbents. A Supramolecular Perspective. *Ind. Eng. Chem. Res.* **2019**, *58*, 14761−14774.

(21) Ortega, G.; Briceño, A. Template-stereocontrolled [2+2] Photoreactions Directed by Surface Recognition on Hydrophilic Functionalized Carbon Materials. *Cryst. Eng. Comm.* **2018**, *20*, 2932−2939.

(22) Badjić, J. D.; Nelson, A.; Cantrill, S. J.; Turnbull, W. B.; Stoddart, J. F. Multivalency and Cooperativity in Supramolecular Chemistry. *Acc. Chem. Res.* **2005**, *38*, 723−732.

(23) Fasting, C.; Schalley, C. A.; Weber, M.; Seitz, O.; Hecht, S.; Koksch, B.; Dernedde, J.; Graf, C.; Knapp, E.-W.; Haag, R. Multivalency as a Chemical Organization and Action Principle. *Angew. Chem., Int. Ed.* **2012**, *51*, 10472−10498.

(24) Haag, R. Multivalency as a chemical organization and action principle. *Beilstein J. Org. Chem.* **2015**, *11*, 848−849.

(25) Briceño, A.; Escalona, A. M. Exploiting the Use of Multivalent Interactions in the Design of Photoreactive Supramolecular Assemblies. From Solution to Crystal Engineering. In *Photochemistry*; Fasani, E.; Albini, A., Eds.; RSC Publishing Cambridge: U.K., 2016; Vol. *43*, pp 286−329.

(26) Chiang, R.-T.; Chiang, R.-K.; Shieu, F.-S. Hydrophilic hollow carbon nanocapsules for high-capacity adsorptive removal of cationic dyes in aqueous systems. *RSC Adv.* **2015**, *5*, 6123−6130.

(27) Hu, B.; Yu, S. H.; Wang, K.; Liu, L.; Xu, X. W. Functional Carbonaceous Materials from Hydrothermal Carbonization of Biomass: An Effective Chemical Process. *Dalton Trans.* **2008**, *40*, 5414−5423.
(28) Titirici, M. M.; White, R. J.; Brun, N.; Budarin, V. L.; Su, D. S.; del Monte, F.; Clark, J. H.; MacLachlan, M. Sustainable Carbon Materials. *Chem. Soc. Rev.* **2015**, *44*, 250−290.
(29) Skubiszewska-Zięba, J.; Sydorchuk, V. V.; Guņ'ko, V. M.; Leboda, R. Hydrothermal Modification of Carbon Adsorbents. *Adsorption* **2011**, *17*, 919−927.
(30) Zhao, R.; Wang, Y.; Li, X.; Sun, B.; Li, Y.; Ji, H.; Qiu, J.; Wang, C. Surface Activated Hydrothermal Carbon-Coated Electrospun PAN Fiber Membrane with Enhanced Adsorption Properties for Herbicide. *ACS Sustainable Chem. Eng.* **2016**, *4*, 2584−2592.
(31) Qiao, M.; Meysami, S. S.; Ferrero, G. A.; Xie, F.; Meng, H.; Grobert, N.; Titirici, M.-M. Low-Cost Chitosan-Derived N-Doped Carbons Boost Electrocatalytic Activity of Multiwall Carbon Nanotubes. *Adv. Funct. Mater.* **2018**, *28*, No. 1707284.
(32) Ahlawat, W.; Kataria, N.; Dilbaghi, N.; Hassan, A. A.; Kumar, S.; Kim, K.-H. Carbonaceous Nanomaterials as Effective and Efficient Platforms for Removal of Dyes from Aqueous Systems. *Environ. Res.* **2020**, *181*, No. 108904.
(33) Machado, F. M.; Bergmann, C. P.; Lima, E. C.; Royer, B.; de Souza, F. E.; Jauris, I. M.; Calvete, T.; Fagan, S. B. Adsorption of Reactive Blue 4 Dye from Water Solutions by Carbon Nanotubes: Experiment and Theory. *Phys. Chem. Chem. Phys.* **2012**, *14*, 11139−11153.
(34) Desiraju, G. R. Supramolecular Synthons in Crystal Engineering-A New Organic Synthesis. *Angew. Chem., Int. Ed.* **1995**, *34*, 2311−2327.
(35) MacGillivray, L. R. Organic Synthesis in the Solid State via Hydrogen-Bond-Driven Self-Assembly. *J. Org. Chem.* **2008**, *73*, 3311−3317.
(36) Ma, J. C.; Dougherty, D. A. The Interaction Cation-π. *Chem. Rev.* **1997**, *97*, 1303−1324.
(37) She, N.; Moncelet, D.; Gilberg, L.; Lu, X.; Sindelar, V.; Briken, V.; Isaacs, L. Glycoluril-Derived Molecular Clips are Potent and Selective Receptors for Cationic Dyes in Water. *Chem. - Eur. J.* **2016**, *22*, 15270−15279.
(38) Karousis, N.; Tagmatarchis, N.; Tasis, D. Current Progress on the Chemical Modification of Carbon Nanotubes. *Chem. Rev.* **2010**, *110*, 5366−5397.
(39) Hernandez, V.; Arevalo, J.; Plaza, E.; Diaz, L.; Sosa, E.; Morales, R.; Atencio, R. Purification of MWCNT and its characterization by scanning electron microscopy and thermogravimetric analysis. *Acta Microsc.* **2013**, *22*, 256−261.
(40) Kosmulski, M. *Surface Charging and Points of Zero Charge*; CRC: Boca Raton, FL, 2009.
(41) Boehm, H. P. Surface Oxides on Carbon and their Analysis: A Critical Assessment. *Carbon* **2002**, *40*, 145−149.
(42) Sing, K. S. W. Reporting physisorption data for gas/solid systems with special reference to the determination of surface area and porosity (Recommendations 1984). *Pure Appl. Chem.* **1985**, *57*, 603−619.
(43) Thommes, M.; Kaneko, K.; Neimark, A. V.; Olivier, J. P.; Rodriguez-Reinoso, F.; Rouquerol, J.; Sing, K. S. W. Physisorption of gases, with special reference to the evaluation of surface area and pore size distribution (IUPAC Technical Report). *Pure Appl. Chem.* **2015**, *87*, 1051−1069.
(44) Cárdenas-Aguiar, E.; Gascó, G.; Paz-Ferreiro, J.; Méndez, A. Thermogravimetric analysis and carbon stability of chars produced from slow pyrolysis and hydrothermal carbonization of manure waste. *J. Anal. Appl. Pyrolysis* **2019**, *140*, 434−443.
(45) Yudianti, R.; Onggo, H.; Sudirman; Saito, Y.; Iwata, T.; Azuma, J. Analysis of Functional Group Sited on Multi-Wall Carbon Nanotube Surface. *Open Mater. Sci.* **2011**, *5*, 242−247.
(46) Silva, W. M.; Ribeiro, H.; Seara, L.; Calado, H.; Ferlauto, A.; Paniago, R.; Leite, C.; Silva, G. Surface properties of oxidized and aminated multi-walled carbon nanotubes. *J. Braz. Chem. Soc.* **2012**, *23*, 1078−1086.
(47) Frontera, A.; Gamez, P.; Mascal, M.; Mooibroek, T. J.; Reedijk, J. Putting Anion−π Interactions Into Perspective. *Angew. Chem., Int. Ed.* **2011**, *50*, 9564−9583.
(48) Qi, Z.-P.; Yang, J.-M.; Kang, Y.-S.; Guo, F.; Sun, W.-Y. Facile water-stability evaluation of metal−organic frameworks and the property of selective removal of dyes from aqueous solution. *Dalton Trans.* **2016**, *45*, 8753−8759.
(49) Rafatullah, M.; Sulaiman, O.; Hashim, R.; Ahmad, A. Adsorption of methylene blue on low-cost adsorbents: a review. *J. Hazard. Mater.* **2010**, *177*, 70−80.
(50) Wang, M.; Song, X.-x.; Cheng, X.-L.; Zhou, X.; Zhang, X.-f.; Cai, Z.; Xu, Y.-M.; Gao, S.; Zhao, H.; Huo, L.-H. Highly selective and efficient adsorption dyes self-assembled by 3D hierarchical architecture of molybdenum oxide. *RSC Adv.* **2015**, *5*, 85248−85255.
(51) Parmar, B.; Bisht, K. K.; Rajput, G.; Suresh, E. Recent advances in metal−organic frameworks as adsorbent materials for hazardous dye molecules. *Dalton Trans.* **2021**, *50*, 3083−3108.
(52) Khan, M. S.; Khalid, M.; Shahid, M. What triggers dye adsorption by metal organic frameworks? The current perspectives. *Mater. Adv.* **2020**, *1*, 1575−1601.
(53) Shi, Y.; Chang, Q.; Zhang, T.; Song, G.; Sun, Y.; Ding, G. A review on selective dye adsorption by different mechanisms. *J. Environ. Chem. Eng.* **2022**, *10*, No. 108639.

https://doi.org/10.1021/acsomega.2c08203
ACS Omega 2023, 8, 11233−11250